



Article

# BTEAC Catalyzed Ultrasonic-Assisted Synthesis of Bromobenzofuran-Oxadiazoles: Unravelling Anti-HepG-2 Cancer Therapeutic Potential through In Vitro and In Silico Studies

Ali Irfan <sup>1</sup>, Ameer Fawad Zahoor <sup>1,\*</sup>, Azhar Rasul <sup>2</sup>, Sami A. Al-Hussain <sup>3</sup>, Shah Faisal <sup>4</sup>, Sajjad Ahmad <sup>5</sup>, Rida Noor <sup>1</sup>, Muhammed Tilahun Muhammed <sup>6</sup> and Magdi E. A. Zaki <sup>3,\*</sup>

<sup>1</sup> Department of Chemistry, Government College University Faisalabad, Faisalabad 38000, Pakistan

<sup>2</sup> Department of Zoology, Government College University Faisalabad, Faisalabad 38000, Pakistan

<sup>3</sup> Department of Chemistry, College of Science, Imam Mohammad Ibn Saud Islamic University (IMSIU), Riyadh 11623, Saudi Arabia

<sup>4</sup> Department of Chemistry, Islamia College University Peshawar, Peshawar 25120, Pakistan

<sup>5</sup> Department of Health and Biological Sciences, Abasyn University, Peshawar 25000, Pakistan

<sup>6</sup> Department of Pharmaceutical Chemistry, Faculty of Pharmacy, Suleyman Demirel University, Isparta 32260, Turkey

\* Correspondence: fawad.zahoor@gmail.com (A.F.Z.); mezaki@imamu.edu.sa (M.E.A.Z.); Tel.: +92-333-672-9186 (A.F.Z.)



**Citation:** Irfan, A.; Zahoor, A.F.; Rasul, A.; Al-Hussain, S.A.; Faisal, S.; Ahmad, S.; Noor, R.; Muhammed, M.T.; Zaki, M.E.A. BTEAC Catalyzed Ultrasonic-Assisted Synthesis of Bromobenzofuran-Oxadiazoles: Unravelling Anti-HepG-2 Cancer Therapeutic Potential through In Vitro and In Silico Studies. *Int. J. Mol. Sci.* **2023**, *24*, 3008. <https://doi.org/10.3390/ijms24033008>

Academic Editors: Kalevi Kairemo and Pritam Sadhukhan

Received: 14 December 2022

Revised: 11 January 2023

Accepted: 13 January 2023

Published: 3 February 2023



**Copyright:** © 2023 by the authors. Licensee MDPI, Basel, Switzerland. This article is an open access article distributed under the terms and conditions of the Creative Commons Attribution (CC BY) license (<https://creativecommons.org/licenses/by/4.0/>).

**Abstract:** In this work, BTEAC (benzyl triethylammonium chloride) was employed as a phase transfer catalyst in an improved synthesis (up to 88% yield) of S-alkylated bromobenzofuran-oxadiazole scaffolds **BF1-9**. These bromobenzofuran-oxadiazole structural hybrids **BF1-9** were evaluated in vitro against anti-hepatocellular cancer (HepG2) cell line as well as for their in silico therapeutic potential against six key cancer targets, such as EGFR, PI3K, mTOR, GSK-3 $\beta$ , AKT, and Tubulin polymerization enzymes. Bromobenzofuran structural motifs **BF-2**, **BF-5**, and **BF-6** displayed the best anti-cancer potential and with the least cell viabilities ( $12.72 \pm 2.23\%$ ,  $10.41 \pm 0.66\%$ , and  $13.08 \pm 1.08\%$ ), respectively, against HepG2 liver cancer cell line, and they also showed excellent molecular docking scores against EGFR, PI3K, mTOR, and Tubulin polymerization enzymes, which are major cancer targets. Bromobenzofuran-oxadiazoles **BF-2**, **BF-5**, and **BF-6** displayed excellent binding affinities with the active sites of EGFR, PI3K, mTOR, and Tubulin polymerization enzymes in the molecular docking studies as well as in MMGBSA and MM-PBSA studies. The stable bindings of these structural hybrids **BF-2**, **BF-5**, and **BF-6** with the enzyme targets EGFR and PI3K were further confirmed by molecular dynamic simulations. These investigations revealed that 2,5-dimethoxy-based bromobenzofuran-oxadiazole **BF-5** ( $10.41 \pm 0.66\%$  cell viability) exhibited excellent cytotoxic therapeutic efficacy. Moreover, computational studies also suggested that the EGFR, PI3K, mTOR, and Tubulin polymerization enzymes were the probable targets of this **BF-5** scaffold. In silico approaches, such as molecular docking, molecular dynamics simulations, and DFT studies, displayed excellent association with the experimental biological data of bromobenzofuran-oxadiazoles **BF1-9**. Thus, in silico and in vitro results anticipate that the synthesized bromobenzofuran-oxadiazole hybrid **BF-5** possesses prominent anti-liver cancer inhibitory effects and can be used as lead for further investigation for anti-HepG2 liver cancer therapy.

**Keywords:** bromobenzofuran-oxadiazole; BTEAC; HepG-2 cell line; EGFR; PI3K, mTOR and tubulin polymerization inhibitors; SAR; molecular docking; MD simulations; DFT studies

## 1. Introduction

Cancer is a serious threat to today's world and is considered the second foremost cause of death globally. The search for new anticancer therapeutic agents has gained

considerable attention and interest. Many research groups of synthetic/medicinal chemists and pharmacologists are working to discover and develop novel anticancer agents for the treatment of around 100 different types of cancers [1–4]. Liver cancer is the fourth most common cause of deaths among all the cancers, and it is the seventh leading cause of death in women and the fifth in men worldwide. According to the statistics, liver disease will become a global problem by 2025, affecting almost one million people across the world. The major cause of hepatocellular carcinoma (HCC) is obesity, hepatitis C and B viruses (HCV & HBV), diabetes, and alcoholic and nonalcoholic fatty liver diseases (AFLD & NAFLD) [5–9]. Various treatments are in practice to treat cancerous cells; 49% of cancer cells are treated with surgery, 40% with radiotherapy, and only 11% are being cured with chemotherapy.

Various chemotherapeutics are available to cure different cancers, yet most of them suffer from certain drawbacks (being expensive, often having less efficacy than required, and carrying a lot of negative side effects) [10–13]. The development of new bioactive privileged structural motifs based on molecular recognition is the core and significant objective of medicinal chemistry. The oxygen and nitrogen containing heterocycles have always been of great synthetic/biological interest owing to their broad spectrum of applications in the fields of medicinal chemistry, pharmaceuticals, and pharmacology. The compound's structures innately lock the therapeutic potential against various diseases and diversified structures of heterocyclic scaffolds are the main dynamic source to act as biologically active therapeutics. Therapeutically, the heterocyclic oxadiazole is the one of the most famous pharmacophores of oxygen and nitrogen, containing a five member azole family that is an integral structural unit of various clinical drugs, as displayed in Figure 1. In general, the biological properties manifested by oxadiazole moiety bearing molecules include anti-fungal, anti-inflammatory, analgesic, anti-diabetic, anticancer, antibacterial, antiviral, antibacterial, antitumor, hypotensive, anti-obesity, etc. [14–19].

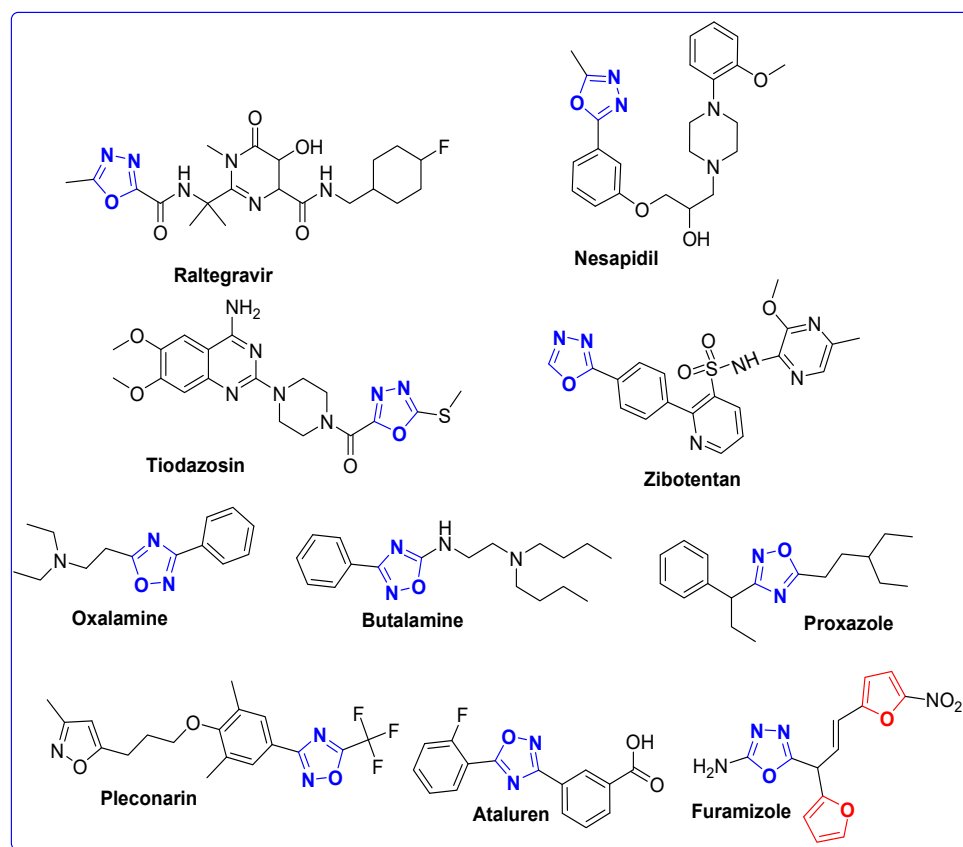


**Figure 1.** The most famous oxadiazole core-based clinical drugs.

As per recent literature, benzofuran derivatives also exhibit a wide spectrum of versatile biological activities, such as a bone anabolic agent, anti-inflammatory, antimicrobial agents, monoamine oxidase (MAO) inhibitors, tumor necrosis factor- $\alpha$  (TNF- $\alpha$ ) inhibitors, anti-HIV/HCV, CNS related disorders, antipyretic, renal disorders, anticoagulant, anti-lung cancer, dual active ligands of 5-HT<sub>1A</sub> and serotonin reuptake inhibitors, anti-TB, farnesyltransferase (FTase) inhibitors, aromatase (cytochrome P450) inhibitors, Pim-1 serine/threonine-protein kinase inhibitors, hypoxia-inducible factor (HIF-1 $\alpha$ ) inhibitors, serotonin receptor inhibitors (5-HT<sub>1A</sub>), glycogen synthase kinase (GSK-3 $\beta$ ) inhibitors, mammalian target of the rapamycin (mTOR) inhibitors, prolyl endopeptidase inhibitors (PEP), cholinesterase activity inhibitors,  $\alpha$ -glucosidase inhibitors, tubulin polymerization inhibitors, anti-human liver carcinoma cell line (HepG2), serine-threonine kinase (AKT) inhibitors, PLK1 PBD inhibitors, PI3K/Akt inhibitors and VEGFR-2 tyrosine kinase inhibitors, etc. Some of the most famous benzofuran core based clinically active therapeutics have been depicted in Figure 2 [20–27].

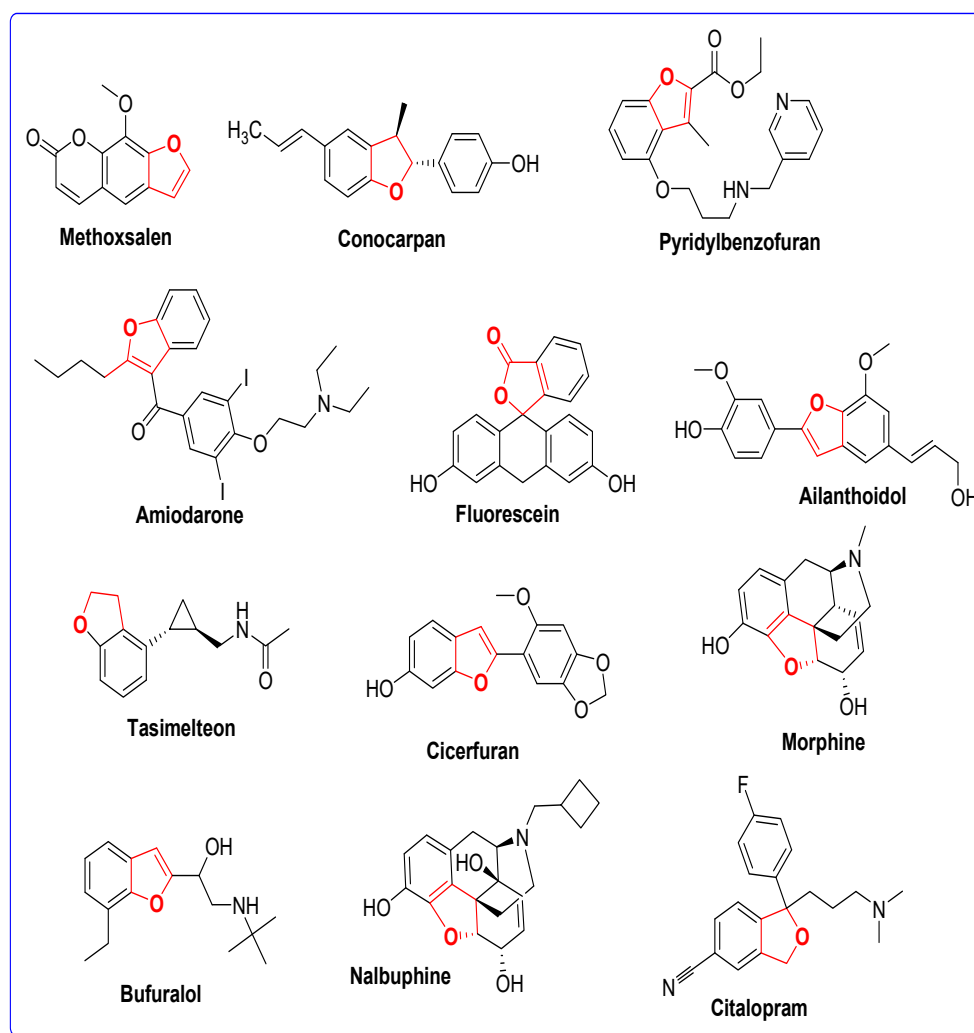


**Figure 2.** Some of the most famous benzofuran core-based clinical drugs.

#### *The Rationale of Molecular Design of Bromobenzofuran-oxadiazoles BF1-9 against HepG2 Cancer Cell Line*

The versatile therapeutic potential of oxadiazoles has made this moiety an important pharmacological scaffold for drug design, especially in the field of oncology [28,29]. A large library of oxadiazoles, such as naproxen-, benzoxazole-, piperazinyl-, thienyl-, and naphthalene-based oxadiazoles and 2,5-disubstituted-1,3,4-oxadiazoles, etc. displayed

excellent anti-cancer potential against HepG2 cell line (Figure 3). Benzofuran analogues, such as thiazole-based benzofurans, have been found to be more active scaffolds than the standard drug 5-fluorouracil. Furan-thiazole based oxadiazoles displayed comparable IC<sub>50</sub> values to the reference drug doxorubicin. Similarly, trifluoro containing benzofuran hybrids exhibited strong anti-proliferative efficacy against HepG-2 cell line as displayed in Figure 3 [24,30–34].

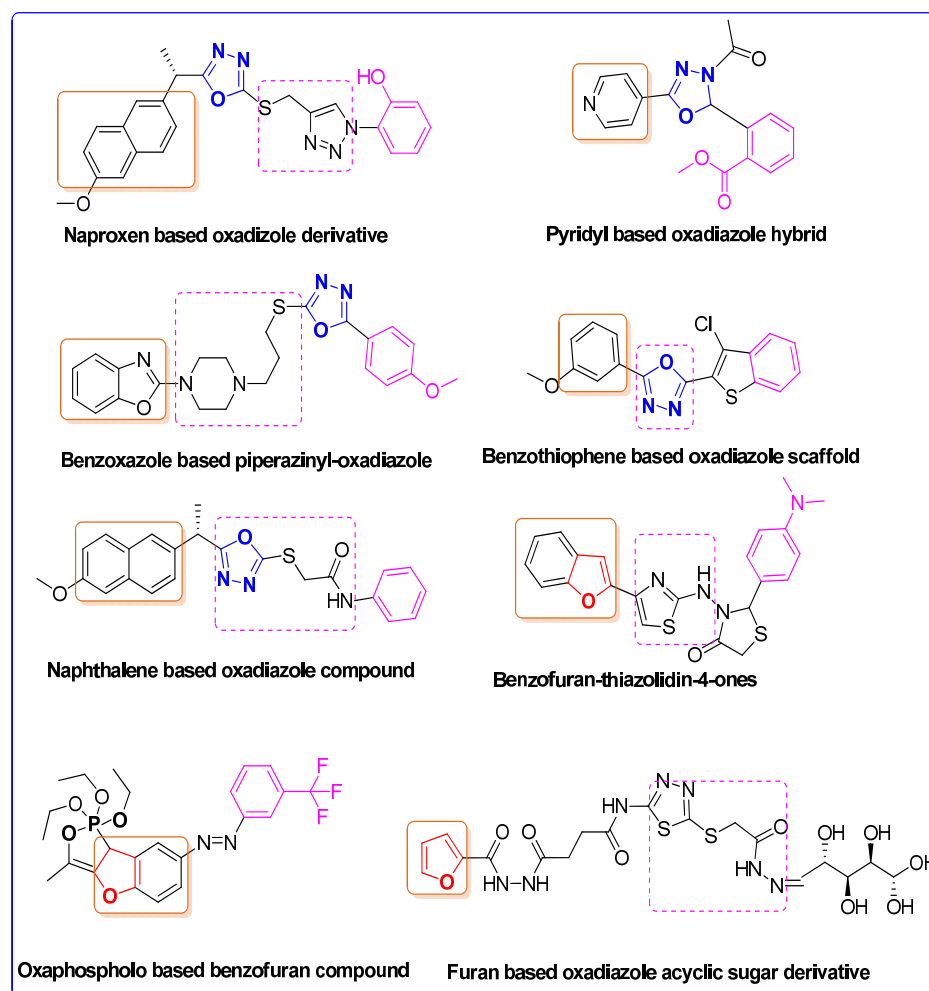


**Figure 3.** The most active furan and oxadiazole core-based anti-HepG-2 hybrids.

The rationale of the current study was based on the molecular hybridization of bromo-arylated fragment with the combination of two major bioactive heterocyclic moieties furan and oxadiazole, each of which possess excellent and privileged pharmaceutical and pharmacological profiles, as demonstrated in Figures 1–3, respectively. In the recent research work, we screened the synthesized substituted *S*-arylated benzofuran-oxadiazole scaffolds against the HepG-2 cancer cell line.

Based on the plethora of the research cited above, we were interested to assess the therapeutic potential of bromobenzofuran-oxadiazoles **BF1-9** as anti-hepatic cancer agents.

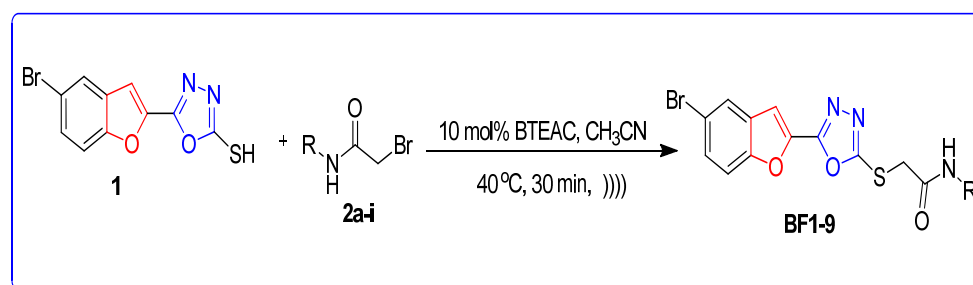
## 2. Materials and Methods

### 2.1. Materials for the Synthesis Bromobenzofuran-Oxadiazole Derivatives **BF1-9**

The ultrasonic irradiated experimental synthetic strategy was performed in a 1.9-L capacity ultrasonic cleaner bath (model 1510) powered by a 115 V heater switch, 47 kHz, and mechanical timer. In this study, all analytical grade starting materials, reagents, and solvents were purchased from Alfa Aesar or Sigma Aldrich. The reactions were monitored by thin-layer chromatography (TLC) using aluminum-backed silica gel plates.

## 2.2. BTEAC Catalyzed Synthesis of Bromobenzofuran-Oxadiazole Structural Hybrids **BF1-9** by Ultrasonic Irradiated Synthetic Approach

A reaction mixture containing bromobenzofuran-oxadiazole-2-thiol **1** (1 mmol) [35,36], BTEAC (10 mol%), and substituted bromoacetanilide derivatives **2a-i** (1.2 mmol) [35,36] in CH<sub>3</sub>CN was sonicated for 30 min at 40 °C (Scheme 1). Upon reaction completion, n-hexane was added to afford *S*-arylated bromobenzofuran-oxadiazole derivatives **BF1-9** as precipitates, which were further purified with an ethanolic recrystallization process or column chromatography technique using ethyl acetate–petroleum ether (1:9) [37–39].



**Scheme 1.** BTEAC catalyzed Ultrasonic assisted synthesis of *S*-alkylated bromobenzofuran-oxadiazole structural hybrids **BF1-9**.

## 2.3. Anti-hepatocellular Carcinoma MTT Assay

The anti-hepatocellular therapeutic potential of the afforded bromobenzofuran-oxadiazoles **BF1-9** was evaluated by applying the MTT assay, and these structural hybrids **BF1-9** were screened against the HepG2 cancer cell line [40,41]. The Dulbecco's modified Eagle's medium was used to develop the HepG2 cell line as a monolayer culture composed of 10% FBS, 100 µg/mL penicillin, and 1% streptomycin. The humid atmosphere at 37 °C was provided for incubation, which consisted of 95% air, 5% CO<sub>2</sub>, and water. The synthesized bromobenzofuran-oxadiazoles **BF1-9** (100 µg/100 mL) were dissolved in DMSO to treat the HepG2 cancer cell line and the DMSO-treated cells were used as a negative control. The 96-well plates were used to culture HepG2 cells overnight, which were further treated with the **BF1-9** compounds.

After the incubation of 48 h, 10 µL, 5 mg/mL of MTT reagent was added to each plate and incubated for 4 h at 37 °C. The percentage cell viability was calculated by measuring the absorbance at 490 nm after the addition of 150 µL DMSO to each plate via a micro-plate reader.

## 2.4. Computational Approach of Bromobenzofuran-Oxadiazoles **BF1-9**

### 2.4.1. Retrieval of EGFR, PI3K, mTOR, AKT, Tubulin Polymerization, and GSK-3β Protein PDB Structures

For the computational investigations, the target enzymes EGFR, PI3K, mTOR, AKT, Tubulin polymerization and GSK-3β protein PDB structures were retrieved from the RCSB with PDB identifiers 4HJO, 3ML9, and 6Y9R [42–45] and 3QKL, 4JSX, and 4O2B [46–48].

### 2.4.2. Designing of Ligands and Molecular Docking of Bromobenzofuran-Oxadiazoles **BF1-9**

The Molecular Operating Environment (MOE) 2009.10 was used to carry out the molecular docking analyses. The Biovia DS software was used to prepare the EGFR, PI3K, mTOR, AKT, Tubulin polymerization, and GSK-3β enzyme protein structures for docking experiments by removing any extra water molecules and heteroatoms from their protein PDB structures. The chemdraw professional program was used to prepare the structures of the ligands **BF-2**, **BF-5**, and **BF-6** and saved them in the mol format for later research [49–52]. The ligand structures were loaded into the MOE before docking, and the MMFF94x forcefield was used to reduce their energy. The protein PDBs was opened in MOE and three d-protonated using the MMFF94x force field. The active site of the six proteins

was located and selected using the Site Finder function of MOE. Using the Triangle Matcher placement techniques, the compounds were docked in the binding pocket and scored by the Dock module using the London-dG scoring function of MOE. The ligand-protein interaction was viewed using the Biovia DS Studio software.

#### 2.4.3. ADMET and Drug-Likeness Studies of Bromobenzofuran-Oxadiazoles **BF1-9**

The Swissadme and ADMETlabonline servers were used for the ADME and drug-likeness research, whereas the admetSARonline server was used for toxicity investigations [53–56].

#### 2.4.4. Molecular Dynamic Simulation of Bromobenzofuran-oxadiazoles **BF-2**, **BF-5**, and **BF-6**

The molecular dynamic simulation was done using AMBER20. Preprocessing of the docked complexes was done via the Antechamber program. The receptors and compounds were processed through FF14SB and GAFF force fields, respectively. The systems were energy minimized for 1500 steps. First, the steepest descent followed by conjugate gradient algorithm was used. Heating was done for 310 K in gradual fashion. The systems were equilibrated and then subjected to production run of 50 ns. The CPPTRAJ module was used for trajectories analysis while XMGRACE was applied for making plots. The MMPBSA.py module was used for binding free energies analysis. In total, 1000 frames were picked for MMPBSA and MMGBSA analyses [57–63].

#### 2.4.5. DFT Studies of Bromobenzofuran-Oxadiazoles **BF-2**, **BF-5**, and **BF-6**

The DFT computations of biologically active bromobenzofuran-oxadiazoles **BF-2**, **BF-5** and **BF-6** structural motifs were performed with Gaussian 09. The geometries of compounds **BF-2**, **BF-5**, and **BF-6** were optimized by using the DFT method with B3LYP in the ground state. The basis set was LANL2DZ. Then, energy calculations of **BF-2**, **BF-5**, and **BF-6** were performed by keeping the DFT optimization setups the same. By the time-dependent DFT method, the total energy, the highest occupied molecular orbital (HOMO) energy, and the lowest unoccupied molecular orbital (LUMO) energy were obtained. Thereafter, the related parameters were computed using these values. The DFT computation results were visualized and analyzed using GaussView 5.0 [64–67].

### 2.5. Statistical Data

The statistical data was analyzed with the Prism software, and the results of the study were measured in triplicates and depicted as mean  $\pm$  SD.

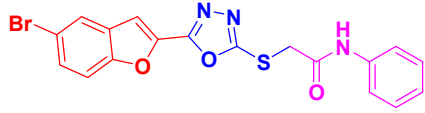
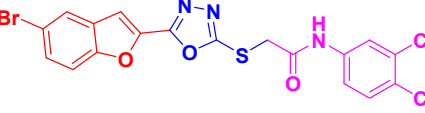
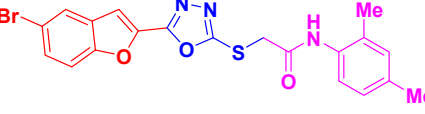
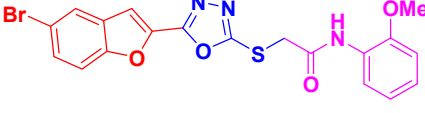
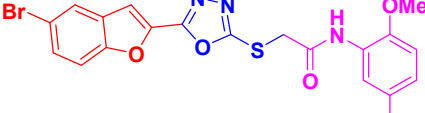
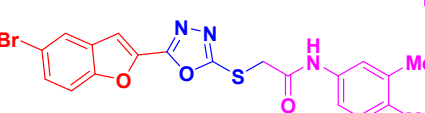
## 3. Results and Discussion

### 3.1. Chemistry

#### Synthesis of Bromobenzofuran-Oxadiazole Structural Hybrids **BF1-9**

In the present research work, BTEAC catalyzed synthetic protocol was applied to furnish substituted 1,3,4-oxadiazole appended bromobenzofuran structural motifs **BF1-9** as sketched in Scheme 1. In the methodology, the scaffold **BF-4** containing electron-donating (ED) methoxy group at ortho positions was achieved in maximum 88% yield while the lowest yield was observed for **BF-8** (75%), having highly electronegative electron withdrawing group chlorine at para position (2-position) on the phenyl ring, as shown in Table 1. This BTEAC-catalyzed synthetic approach provided higher reaction yields as compared to our previously reported methodology yields (53–79%) [39].

**Table 1.** Synthetic data of bromobenzofuran-oxadiazole derivatives **BF1-9**.

Compounds	Products	Percentage Yields		Melting Points (MP) °C	
		This Work (Using BTEAC Catalyst)	Reported [39]	Reported [39]	Found
BF-1		82	204–205	203–204	
BF-2		86	227–228	226–227	
BF-3		80	238–240	239–240	
BF-4		88	177–179	177–178	
BF-5		83	188–190	189–190	
BF-6		76	187–188	186–187	
BF-7		75	197–199	197–198	
BF-8		77	192–193	191–193	
BF-9		80	185–186	185–186	

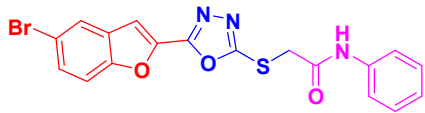
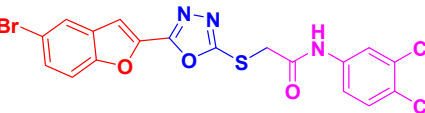
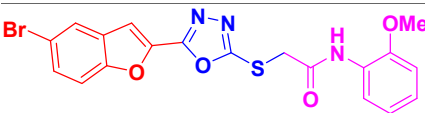
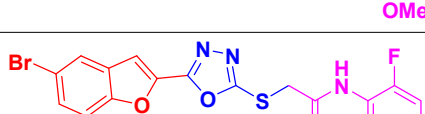
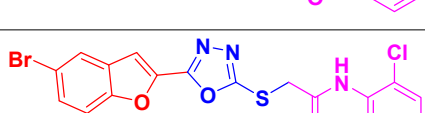
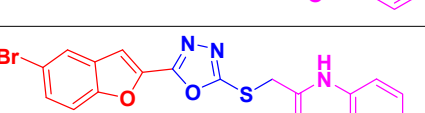
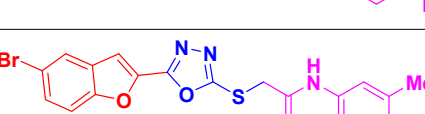
### 3.2. Biological Evaluation of Bromobenzofuran-Oxadiazoles

#### 3.2.1. Anti-Hepatocellular Carcinoma Activity of Bromobenzofuran-Oxadiazoles **BF1-9**

The anti-HepG2 liver cytotoxicity of bromobenzofuran-oxadiazole structural hybrids **BF1-9** was evaluated via MTT assay. The human liver tumor cell line (HepG2) was used to examine one dose-response, and the results are presented in Table 2. These results highlighted the significance of *S*-alkylated bromobenzofuran-oxadiazole derivatives **BF1-9**, which exhibited significant anticancer activity (Cell viability = 10.41 ± 0.66% to 44.69 ± 6.85%). Among all bromobenzofuran-oxadiazole derivatives **BF1-9**, 3,4-dimethylphenyl-containing scaffold **BF-9** showed the maximum cell viability of 44.69 ± 6.85%, which indicated that this structural hybrid **BF-9** is less cytotoxic while 2-methoxyphenyl containing structural motif **BF-4** (13.88 ± 0.6% cell viability) and 4-fluorophenyl-based derivative **BF-8** (13.85 ± 1.08% cell viability) displayed comparable and better cytotoxic potential with respect to the most bioactive bromobenzofuran-oxadiazoles **BF-2**, **BF-5**, and **BF-6**. The phenyl, 2,5-dimethyl phenyl, and 2-chlorophenyl containing bromobenzofuran-oxadiazoles **BF-1**, **BF-3**, and **BF-7** demonstrated moderate anti-hepatic therapeutic efficacies (26.29 ± 17.54% cell viability,

33.12 ± 6.15% cell viability, and 21.47 ± 8.55% cell viability), respectively, as shown in Table 2. As depicted in Table 2, 3,4-Dichloro-based bromobenzofuran-oxadiazole **BF-2**, (12.72 ± 2.23% cell viability), 2-fluorophenyl containing bromobenzofuran-oxadiazole **BF-6** (13.08 ± 1.08% cell viability), and the least cell viability (10.41 ± 0.66%) and maximum anti-hepatic liver cancer therapeutic potential were displayed by 2,4-dimethoxy phenyl based bromobenzofuran-oxadiazole **BF-5**. To evaluate the in-depth therapeutic potential and complete mechanism of inhibition of bromobenzofuran-oxadiazoles **BF1-9** against the human hepatocellular carcinoma (HCC), further in vitro studies on other human HCC tissue cell lines would be necessitated in our further studies by utilizing cell proliferation, apoptosis, and autophagy methodologies.

**Table 2.** Cytotoxic potential of bromobenzofuran-oxadiazole structural hybrids **BF1-9** against HepG2 liver cancer cell line.

Compounds	Products Structure	HepG2 % Cell Viability ± SD
BF-1		26.29 ± 17.54
BF-2		12.72 ± 2.23
BF-3		33.12 ± 6.15
BF-4		13.88 ± 0.6
BF-5		10.41 ± 0.66
BF-6		13.08 ± 1.08
BF-7		21.47 ± 8.55
BF-8		13.85 ± 1.08
BF-9		44.69 ± 6.85
Control	DMSO	100 ± 0

### 3.2.2. Structure-Activity Relationship of Bromobenzofuran-Oxadiazoles **BF1-9**

The newly synthesized bromobenzofuran-oxadiazoles **BF1-9** contained a variety of substituted acetanilides **2a-I**, which were installed to enhance the lipophilicity of the synthesized scaffolds, and the cytotoxic results were prominently improved as mentioned in Table 2. The SAR studies revealed that the substituted acetanilides depicted arbitrary behavior as bromobenzofuran-oxadiazole compounds **BF-2**, **BF-5**, and **BF-6**, which have electron withdrawing 3,4-dichloro, 2,4-dimethoxy, and 2-fluoro groups, showed considerably lower cell viability ( $12.72 \pm 2.23\%$ ,  $10.41 \pm 0.66$ , and  $13.08 \pm 1.08$ ) and highly remarkable and significant anti-cytotoxic potential against HepG2 cancer cells. Bromobenzofuran-oxadiazoles **BF-3** and **BF-9**, which have electron-donating methyl groups at 2,4- and 3,4-positions on phenyl groups of the anilide, resulted in higher cell viability ( $33.12 \pm 6.15\%$  and  $44.69 \pm 6.85\%$ ) and demonstrated the least anticancer therapeutic efficacies as in presented in Table 2. This study indicated that the bromobenzofuran-oxadiazoles having electron-withdrawing methoxy, fluoro, and chloro groups displayed the best and the most significant anticancer therapeutic potential against HepG2 cancer cells than electron-donating methyl group containing benzofuran-oxadiazoles. The cytotoxic therapeutic potential decreased in the following order: 2,5-dimethoxy > 3,4-dichloro > 2-fluoro > 4-fluoro > 2-methoxy > 2-Chloro > Pheny > 2,4-dimethyl > 3,4-dimethyl.

It was observed that the second, fourth and fifth positions of phenyl were responsible for the excellent anti-HepG2 cancer activity of bromobenzofuran-oxadiazoles **BF1-9**, especially of 2,4-dimethoxy containing a **BF-5** derivative. The introduction of electron withdrawing groups (EWG), such as methoxy, fluoro, and chloro on the second, fourth, and fifth positions of phenyl in the bromobenzofuran-oxadiazoles **BF1-9**, enhanced the cytotoxic potential while substituents pattern of the electron donating groups (EDG) on the phenyl of anilide ring decreased the cytotoxic therapeutic potential of bromobenzofuran-oxadiazoles **BF1-9**, as depicted in Figure 4 and Table 2. The effect of different substituents on the phenyl anilide ring displayed a vital role in cytotoxic behavior of bromobenzofuran-oxadiazole structural hybrids **BF1-9**.

### 3.3. Computational Investigations

#### 3.3.1. Molecular Docking Studies of Bromobenzofuran-Oxadiazoles **BF1-9**

Some of the main targets for liver cancer medication development include several different pathways implicated in crucial cancer-related activities like angiogenesis, cell proliferation, and apoptosis. These pathways include several molecular targets that are reported to have uncontrolled expression rates that help in the invasiveness and proliferation of these cancers in the liver. When it comes to creating anti-cancer drugs, some of the important key signaling molecules/molecular targets of interest include the PI3K/Akt/mTOR, tubulin polymerization, GSK-3 $\beta$ , EGFR, and its related pathways [68–74].

In our studies, the in vitro investigations showed that three of the synthesized compounds **BF-2**, **BF-5**, and **BF-6** showed good activities against the HepG2 liver cancer cell line and for the prediction of the probable targets of these synthesized compounds. EGFR performs vital roles in the physiology of epithelial cells and is the target of numerous commonly used medicines to treat cancer in clinical practice since it is commonly mutated and/or overexpressed in various types of human malignancies. Several novel benzofuran scaffolds carrying compounds have been reported in the literature to have significant anti-EGFR activities [75–77]. Similarly, other important cancer molecular targets and their related pathways like PI3K, Akt, GSK-3 $\beta$ , mTOR, and tubulin polymerization, etc. have also been targeted by these types of compounds, and they exhibit good anti-cancer properties against these molecular targets [78–83].

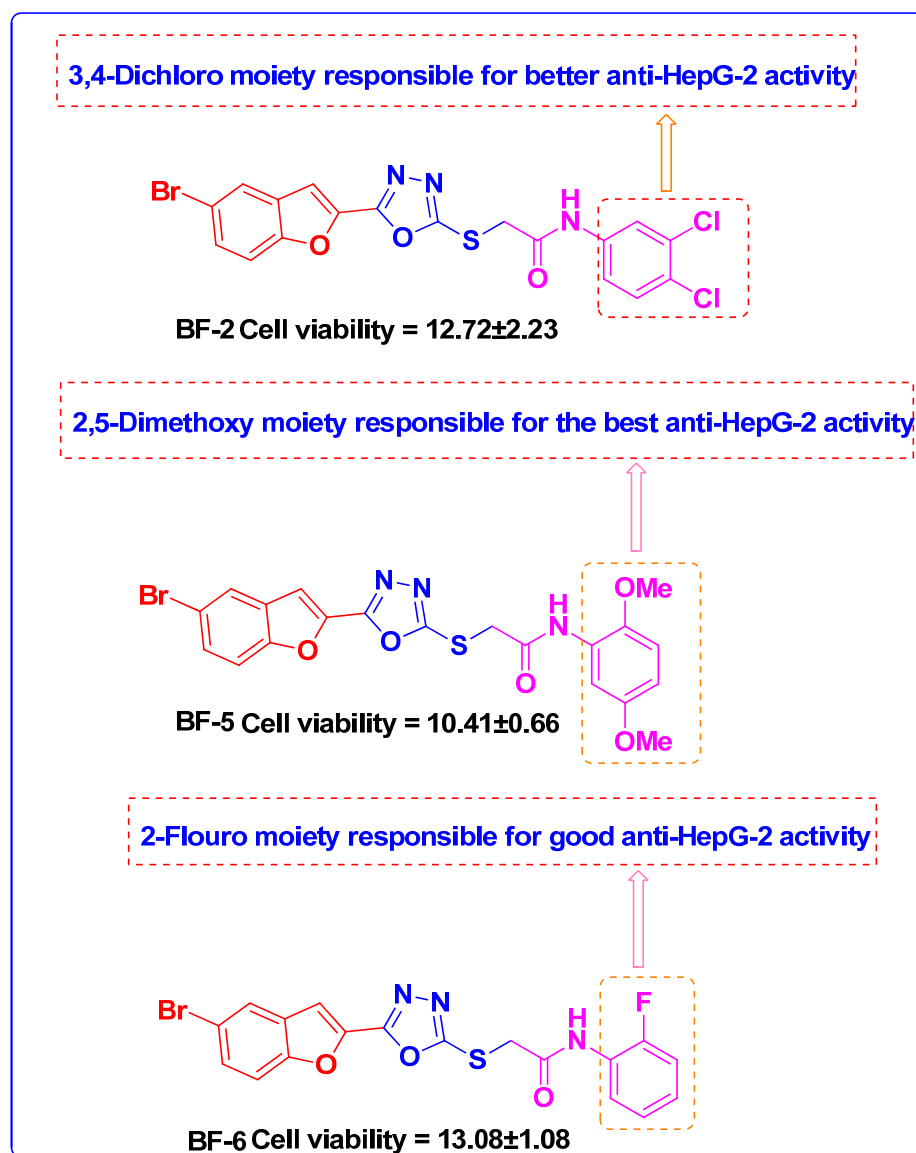


**Figure 4.** The most bio-active anti-HepG-2 bromobenzofuran-oxadiazoles.

Based on these observations, we performed *in silico* investigations of the synthesized bromobenzofuran-oxadiazole compounds against these different cancer-related molecular targets. We exploited molecular docking approaches to evaluate the binding affinities and the interactions of three potent compounds **BF-2**, **BF-5**, and **BF-6** against EGFR, PI3K, Akt, GSK-3 $\beta$ , mTOR, and tubulin polymerization, which are important molecular targets in various cancers.

The investigations of these bromobenzofuran-oxadiazole compounds **BF-2**, **BF-5**, and **BF-6** against the EGFR revealed that the bromobenzofuran-oxadiazole compound **BF-5** showed greater efficacy in the *in vitro* studies; had a binding affinity of  $-15.17$  Kcal/mol with its active site; and made two conventional hydrogen bonds with LYS721, ASP831, and two carbon-hydrogen bonds were observed with the CYS751 and PHE832 of the EGFR active site residues. A single water-assisted hydrogen bond as well as several stabilizing hydrophobic (Pi-sigma, Alkyl, and Pi-Alkyl) interactions were also made by this compound **BF-5** with the active site amino acids of the EGFR enzyme and can be seen in Figure 5.

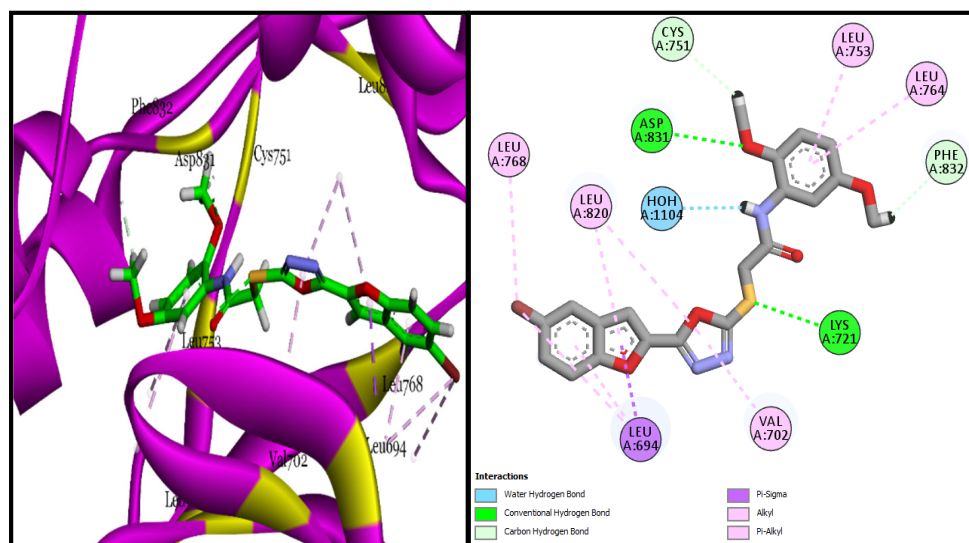


**Figure 5.** Three-dimensional and Two-dimensional interaction images of the **BF-5**+EGFR Protein complex.

Similarly, the other two bromobenzofuran-oxadiazole compounds, **BF-2** and **BF-6**, were able to bind with the active site of the EGFR with binding affinities of  $-14.17$  Kcal/mol and  $-12.59$  Kcal/mol, respectively. These two compounds (**BF-2** and **BF-6**) also made significant interactions of different types by engaging the active site residues of EGFR via multiple hydrogen bonds and halogen interactions. These two bromobenzofuran-oxadiazole derivatives showed multiple hydrophobic stabilizing interactions and can be seen in Figure 6.

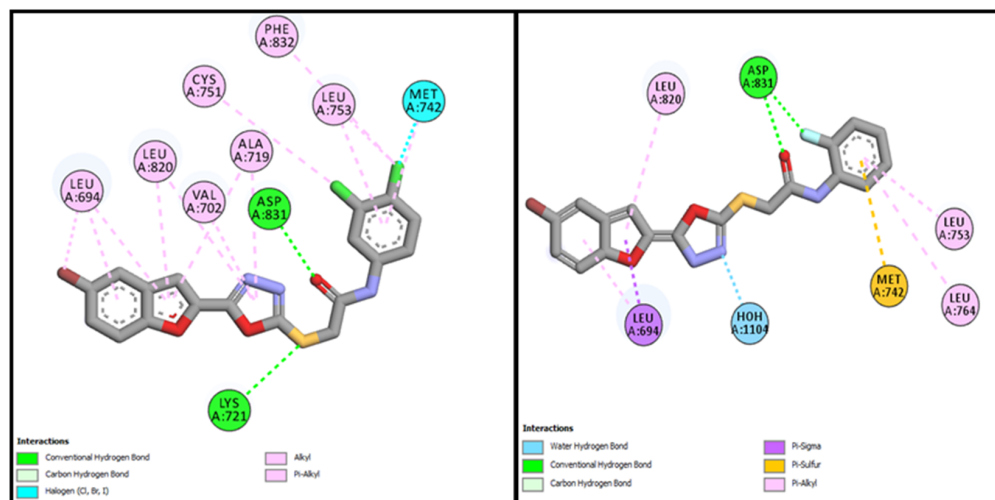


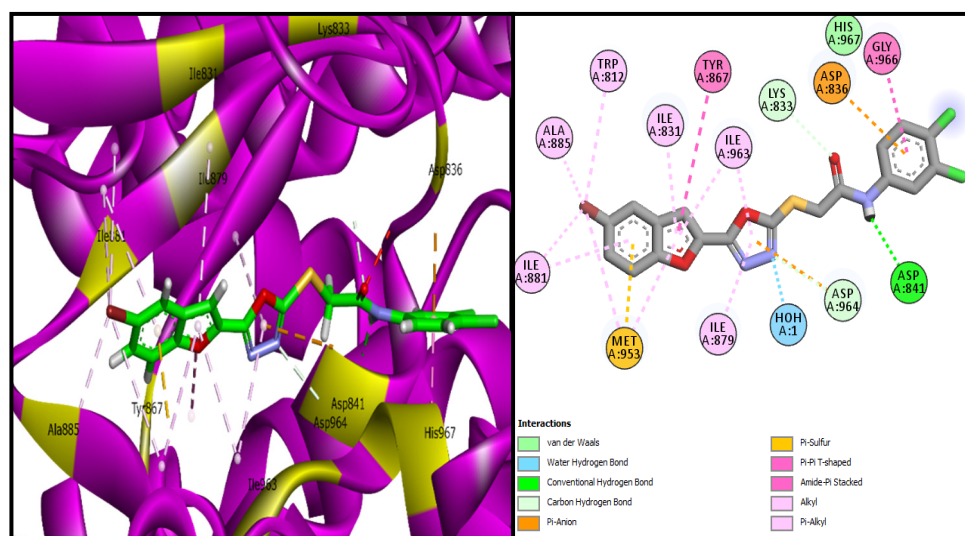
**Figure 6.** Two-dimensional interactive poses of **BF-2** (Left) and **BF-6** (Right) in the EGFR active site.

The docking studies of the standard EGFR Erlotinib inhibitor in these studies showed that Erlotinib bound with the active site of EGFR with a binding affinity of  $-11.67$  Kcal/mol, which suggested that the synthesized novel compounds **BF-2**, **BF-5**, and **BF-6** exhibited higher affinities with EGFR as compared to the standard reference drug Erlotinib. A summary of their binding affinities and their total interactions with the EGFR active site are given in Table 3.

**Table 3.** Binding affinities and other docking parameters of **BF-2**, **BF-5**, and **BF-6** with EGFR.

Compound	Binding Affinity	Interacting Residues	Types of Interactions Made
<b>BF-2</b>	−14.17 Kcal/mol	LEU694, VAL702, ALA719, LYS721, MET742, LEU753, ASP831, CYS751, PHE832	Conventional and Carbon type H-bonds, Halogen interactions, Pi-Alkyl & Alkyl
<b>BF-5</b>	−15.17 Kcal/mol	LEU694, VAL702, LYS721, ASP831, PHE732, CYS751, LEU820, ASP831, PHE832 etc.	H <sub>2</sub> O-Assisted, Conventional and Carbon type H-bonds, Pi-Sigma, Pi-Alkyl & Alkyl
<b>BF-6</b>	−12.59 Kcal/mol	MET742, LEU694, LEU764, LEU753, LEU820	Conventional and Carbon type H-bonds, Pi-Sigma, Pi-Alkyl, Pi-Sulfur
<b>Erlotinib</b>	−11.67 Kcal/mol	LEU694, LYS704, VAL702, ALA719, LYS721, MET769, LEU820	Conventional and Carbon type H-bonds, Pi-Alkyl, Alkyl

Furthermore, we investigated the binding affinities of these three compounds **BF-2**, **BF-5**, and **BF-6** with the PI3K enzyme which is also implicated in various cancer and is an important drug target for bromobenzofuran-based compounds. The docking investigations of **BF-2**, **BF-5**, and **BF-6** revealed that **BF-2** binds with the PI3K active site with the highest binding affinity of −15.17 Kcal/mol. The interaction analysis of its conformational pose inside the PI3K active site showed that **BF-2** made several different types of stronger hydrogen bonds with the PI3K active site (MET953, ASP836, LYS833, ASP964) along with that of water-assisted hydrogen bonding, hydrophobic interactions (Alkyl and Pi-Alkyl) with ALA885, ILE881, ILE879, ILE963, Pi-Sulfur, Pi-Pi T-shaped, and Amide-Pi interaction with the TYR867, GLY966, and Pi-anion as well van der waals interaction was also observed in the **BF-2**+PI3K complex. It can be seen in Figure 7 in three and two dimensional conformations inside the PI3K active site.

**Figure 7.** Three-dimensional and two-dimensional interaction images of the **BF-2**+PI3K protein complex.

The other two lead compounds **BF-5** and **BF-6**, which showed good efficacy in the *in vitro* investigations, also exhibited good binding affinities with the PI3K protein active site. Bromobenzofuran-oxadiazole compound **BF-5** was able to bind with the PI3K active site with a binding affinity of −13.17 Kcal/mol and made water-assisted H-bond and two carbon-hydrogen bonds with the LYS833 and ASP964 active pocket residues; other hydrophobic type interactions, including Pi-Alkyl, Pi-Sigma, Pi-Lone Pair, Pi-Anion, and Pi-Sulfur interactions, were also observed between the **BF-5**+PI3K complex. **BF-6** showed a binding affinity of −12.90 Kcal/mol and showed the same type of multiple types of hydrogen bonding as well water-assisted H-bonding with LYS833 and ASP964 along with other stabilizing hydrophobic, and Amide-Pi stacked interactions with TYR867, GLY966, ASP836, etc. were also observed their two-dimensional interactive diagrams and are given in Figure 8.

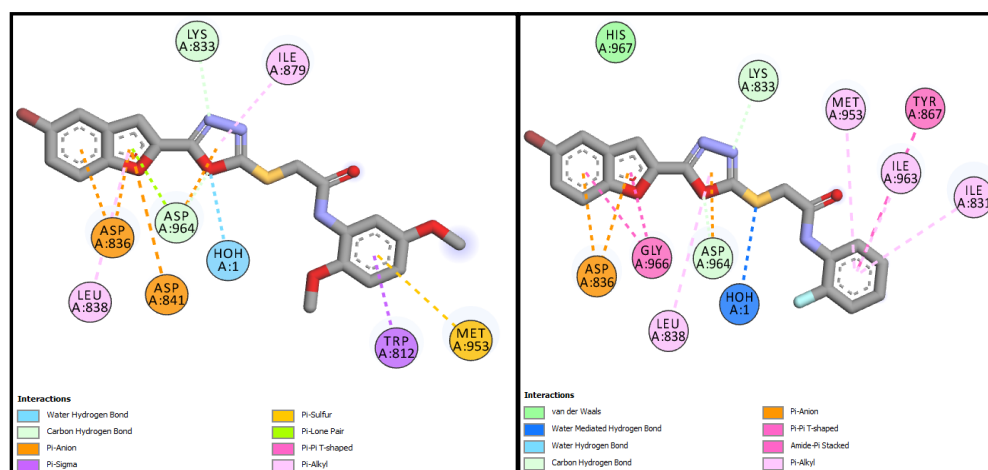


**Figure 8.** Two-dimensional interactive poses of **BF-5** (Left) and **BF-6** (Right) in the PI3K active site.

Overall, three bromobenzofuran-oxadiazoles (**BF-2**, **BF-5**, and **BF-6**) showed stronger binding interactions with the PI3K active site while the Idelalisib standard PI3K inhibitor was able to bind to its active site with a binding affinity of  $-11.42$  Kcal/mol, which suggested that these novel **BF-2**, **BF-5**, and **BF-6** compounds could bind more strongly with the PI3K compared to the standard drugs used in our docking studies. The binding affinity energies of these three (**BF-2**, **BF-5**, and **BF-6**) structural motifs arose due to the interactions of these compounds with the PI3K active pocket amino acid residues and are presented in Table 4.

**Table 4.** Binding affinities and other docking parameters of **BF-2**, **BF-5**, and **BF-6** with PI3K.

Compound	Binding Affinity	Interacting Residues	Types of Interactions Made
<b>BF-2</b>	$-15.17$ Kcal/mol	MET953, ASP836, LYS833, ASP964, ALA885, ILE881, ILE879, ILE963, TYR867, GLY966	H <sub>2</sub> O-Assisted, Conventional and Carbon-H type H-bonds, Halogen interactions, Pi-Alkyl, Alkyl, Pi-Anion, Amide-Pi Stacked, Pi-Sulfur
<b>BF-5</b>	$-13.17$ Kcal/mol	TRP812, LYS833, ASP836, LEU838, ASP841, MET953, ASP964	H <sub>2</sub> O-Assisted, Conventional and Carbon-H type H-bonds, Halogen interactions, Pi-Alkyl, Alkyl, Pi-Anion, Pi-Lone Pair, Amide-Pi Stacked, Pi-Sulfur, etc.
<b>BF-6</b>	$-12.90$ Kcal/mol	MET953, ASP836, LYS833, ASP964, ILE831, ILE963, TYR867, ASP964, GLY966, LEU838	H <sub>2</sub> O-Assisted, Conventional and Carbon-H type H-bonds, Halogen interactions, Pi-Alkyl, Alkyl, Pi-Anion, Amide-Pi Stacked, etc
<b>Idelalisib</b>	$-11.42$ Kcal/mol	MET953, LYS833, ASP964, ILE831, ILE963, TYR867, ASP964, MET804, VAL882	Conventional and Carbon-H type H-bonds and Pi-Donor H-bond, Pi-Alkyl, Alkyl, Pi-Anion, Pi-Pi T-shaped, etc.

Other than these important cancer molecular targets, the bromobenzofuran-oxadiazole compounds **BF-2**, **BF-5**, and **BF-6** were also evaluated via molecular docking studies against the mTOR, AKT, and Tubulin proteins as well because they are also involved in several cancers, and compounds carrying the benzofuran moiety have been reported several times in the literature as potent inhibitors of these proteins. The molecular docking investigations of bromobenzofuran-oxadiazoles **BF-2**, **BF-5**, and **BF-6** against these proteins revealed that out of these three compounds, **BF-5** and **BF-6** showed higher binding affinities with mTOR than the standard mTOR inhibitor (Torin-2) and showed significantly good interactions with its active site. Similarly, docking investigations against the Tubulin protein

showed that **BF-2** and **BF-5** also strongly bind and show good interactions with this protein compared to its standard inhibitor (Colchicine) of Tubulin protein. The binding energies of these compounds against mTOR and Tubulin proteins are given in Table 5, and the two-dimensional diagrams of the best binding compounds against the mTOR and Tubulin proteins are given in Figure 9.

**Table 5.** Binding affinities of **BF-2**, **BF-5**, and **BF-6** with mTOR and Tubulin.

Compound	Binding Affinity with mTOR	Binding Affinity with Tubulin
<b>BF-2</b>	−11.61 kcal/mol	−13.14 kcal/mol
<b>BF-5</b>	−11.84 kcal/mol	−13.79 kcal/mol
<b>BF-6</b>	−11.89 kcal/mol	−10.59 kcal/mol
<b>COLCHICINE Standard against Tubulin</b>	–	−11.85 kcal/mol
<b>TORIN-2 Standard against mTOR</b>	−11.77 kcal/mol	–

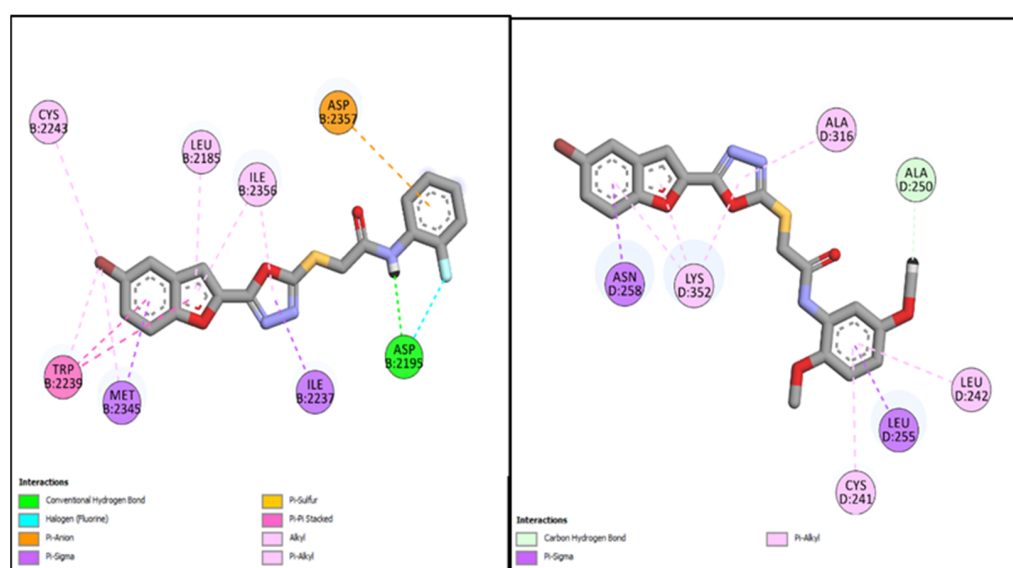


**Figure 9.** Two-dimensional interactive poses of **BF-6** with mTOR (Left) and **BF-5** with Tubulin (Right) in its active sites.

Along with these cancer targets, we also investigated these compounds against the GSK-3 $\beta$  and Akt enzyme, and these studies showed that their binding affinities against the GSK-3 $\beta$  and Akt enzyme were too low compared to the EGFR, PI3K, mTOR, and Tubulin protein molecular targets. Moreover, the computational investigations showed that these compounds bind strongly with the EGFR, PI3K, mTOR, and Tubulin enzymes and have good binding affinities as well as strong interactions, which suggest that these four important cancer-related molecular targets may be the target of these novel bromobenzofuran-oxadiazole compounds.

### 3.3.2. ADMET and Drug-Likeness Studies of Bromobenzofuran-Oxadiazoles **BF1-9**

According to the ADMET assessment (or pharmacokinetics analyses), these bromobenzofuran-oxadiazoles had acceptable lipophilic (iLogP) qualities, good Log S (ESOL) water solubility values, and good human intestine absorptions, and they were designated as HIA+. They were also non-substrates of the P-gp protein, which controls the efflux of substances and medicines from cells through membrane transport. These substances can readily be bio-transformed inside the liver and then be transferred to the excretory organs for excretion from the body because, according to metabolism studies, the findings showed that they are substrates of the crucial metabolic enzyme (CYP450 3A4). The organic cation transporter (OCTs) protein in the kidneys, which is essential for the body's removal of

foreign chemicals and medications, was also not inhibited by these compounds. The toxicity studies of these molecules also showed that they are non-AMES toxic, non-carcinogenic, and non-interferers of the normal function of the T hERG II ion channel, which controls cardiac action potential repolarization. The complete profile of its ADME&T investigations is presented in Table 6 while its structures along with the graphical pharmacokinetic profiles can be seen in Figure 10.

**Table 6.** ADME&T profile of bromobenzofuran-oxadiazoles **BF-2**, **BF-5** and **BF-6**.

Compound	iLogP	LogS	Renal OCTs	AMES Toxicity	BBB+	Carcinogenicity	HIA+
<b>BF-2</b>	3.76	−7.55	Non-inhibitor	None	0.97	None	0.87
<b>BF-5</b>	3.99	−6.56	Non-inhibitor	None	0.97	None	0.87
<b>BF-6</b>	3.41	−6.34	Non-inhibitor	None	0.97	None	0.84

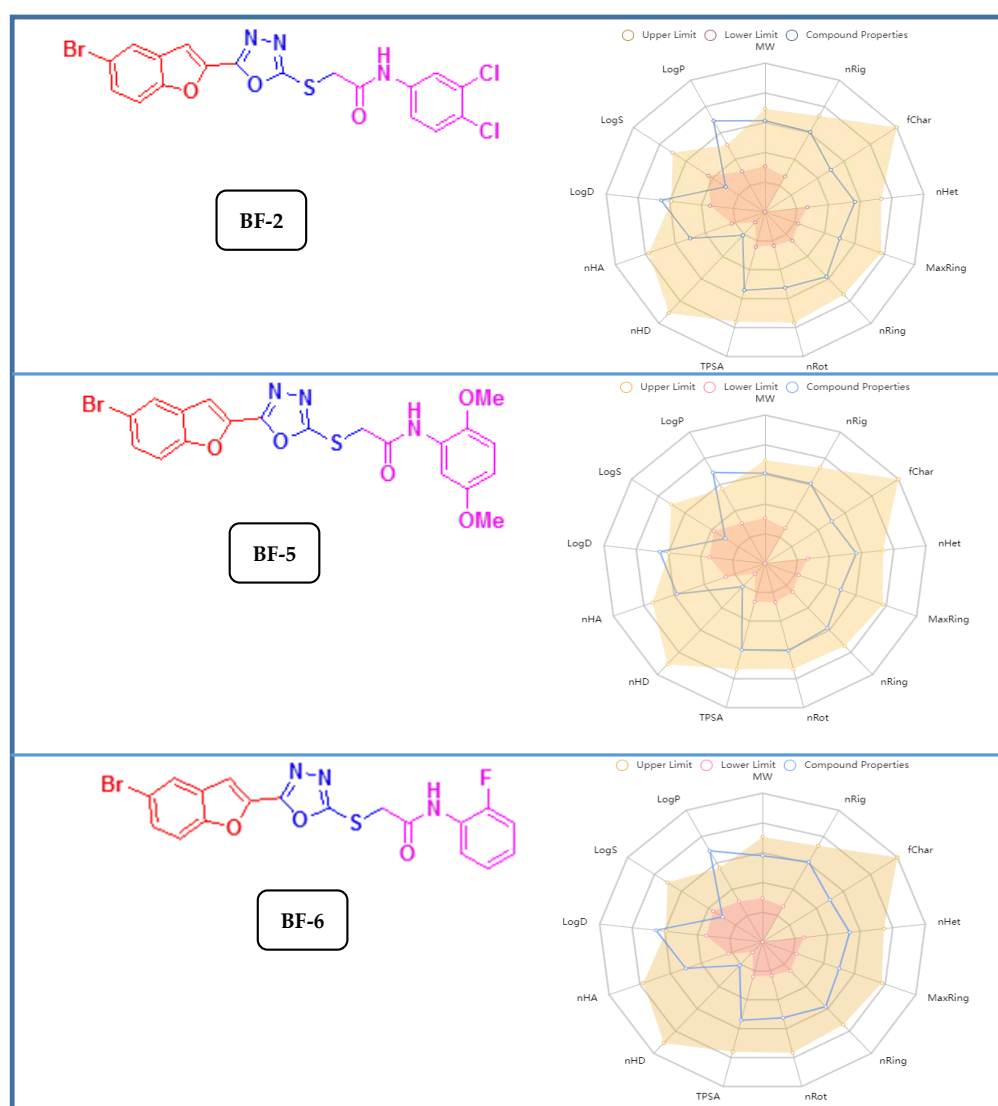


**Figure 10.** Structures and graphical representation of pharmacokinetic profiles of **BF-2**, **BF-5** and **BF-6**.

According to the drug-likeness investigations that involve the identification of the physicochemical attributes and medicinal chemistry of compounds, these bromobenzofuran structural hybrids **BF-2**, **BF-5**, and **BF-6** possessed good topological surface area (TPSA), acceptable molecular weight values, and good synthetic accessibility scores, as shown in

Table 7. These substances adhered to all drug-likeness guidelines, including the Lipinski and Pfizer rules. These substances had good bioavailability scores (greater than 0.10), did not exhibit any PAINS alarms, and obeyed the Golden Triangle rule. The three lead bromobenzofuran-oxadiazole compounds **BF-2**, **BF-5**, and **BF-6** showed noticeably good ADMET and drug-likeness qualities. On the basis of all the investigations analysis, these bromobenzofuran-oxadiazoles leads can safely be developed as potential pharmaceuticals. To evaluate the in depth therapeutic potential and complete mechanism of inhibition of bromobenzofuran-oxadiazoles **BF1-9** against the human hepatocellular carcinoma (HCC), further in vitro studies on other Human HCC tissue cell lines would be necessitated in our further studies by utilizing cell proliferation, apoptosis, and autophagy methodologies.

**Table 7.** Drug-likeness profile of Bromobenzofuran-oxadiazoles **BF-2**, **BF-5** and **BF-6**.

Compounds	Bioavailability Score	PAINS Alerts	Lipinski's Rule	Pfizer Rule	Golden Triangle Rule	TPSA
<b>BF-2</b>	0.55	None	complied	complied	complied	106.46 Å <sup>2</sup>
<b>BF-5</b>	0.55	None	complied	complied	complied	124.92 Å <sup>2</sup>
<b>BF-6</b>	0.55	None	complied	complied	complied	106.46 Å <sup>2</sup>

### 3.3.3. Molecular Dynamic Simulations of Bromobenzofuran-Oxadiazoles **BF1-9**

The dynamics assessment of the most bioactive docked complexes PI3K+**BF-2** and EGFR+**BF-5** were done through a molecular dynamics simulation technique. The simulation trajectories were studied for the structural stability of bromobenzofuran-oxadiazoles with receptors via the root mean square deviation (RMSD), root mean square fluctuation (RMSF), and radius of gyration (RoG). All of these analyses were done based on carbon alpha atoms. Generally, all the analyses predicted the very stable formation of stable complexes. RMSD plots (A part of Figure 11) reported the very stable behavior of the PI3K+**BF-2** complex throughout the simulation time while the EGFR+**BF-5** complex initially experienced some deviation in the first 35 ns. The RMSD of both system maxima touches 4 angstroms. This was also complemented with an RMSF analysis, which complemented the RMSD findings and found the receptors residues in the presence of compounds very stable (B part of Figure 11). The PI3K+**BF-2** complex receptor reported the C-terminal being very flexible compared to the rest of the enzyme structure. The RoG analysis was another confirmation of the RMSD findings and unveiled the systems to have compact nature in the compound's presence.

Binding Free Energy Analysis Further validation of the docking and simulation findings was accomplished using MMGBSA and MMPBSA methods. Both the methods are now frequently used in modern drug discovery as they use modest computational speed and correlate well with the experimental data. The estimated binding free energy results are tabulated in Table 8. As can be seen, both complexes in MMGBSA and MMPBSA are very much stable, as can be understood by  $-38.44$  kcal/mol (MMGBSA) and  $-42.55$  kcal/mol (MMPBSA) for the EGFR+**BF-5** complex and  $-39.54$  kcal/mol (MMGBSA) and  $-45.13$  kcal/mol (MMPBSA) for the PI3K+**BF-2** complex.

The results indicated stable binding conformation of the compounds with the receptors and formed strong intermolecular interactions. The van der Waals and electrostatic energies played a vital role in the complex's stability while a negative contribution was seen from the polar energy component.

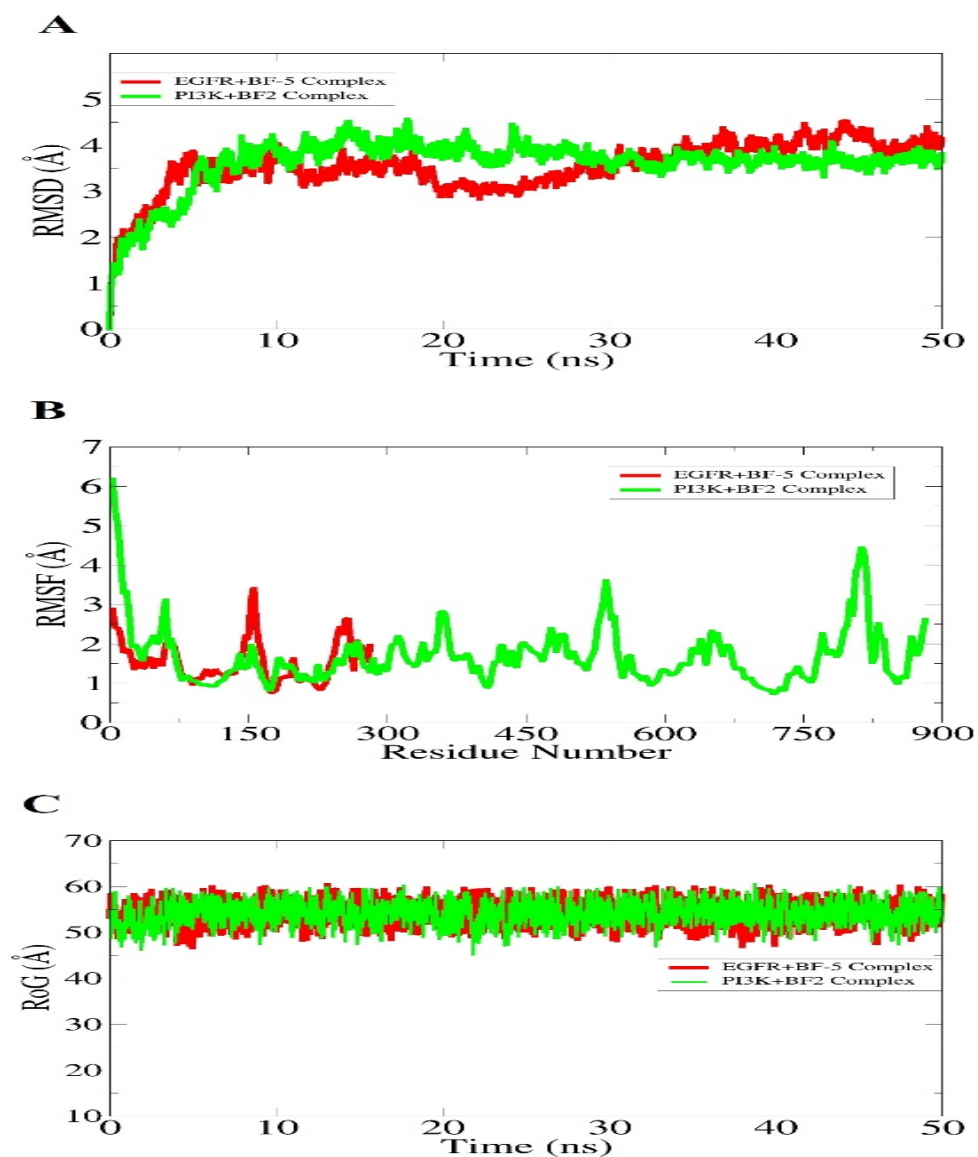


Figure 11. Simulation-based analysis of docked complexes. (A) RMSD (B) RMSF and ROG (C).

Table 8. Binding free energies of complexes in kcal/mol.

Energy Parameter	EGFR+BF-5 Complex	PI3K+BF-2 Complex
	<b>MMGBSA</b>	
Van der Waals	−29.10	−33.90
Electrostatic	−12.20	−10.85
Polar	12.36	11.75
Non-polar	−9.50	−9.55
Delta G gas	−41.3	−44.75
Delta G solv	2.86	2.2
Delta Total	−38.44	−42.55
	<b>MMPBSA</b>	
Van der Waals	−29.10	−33.90
Electrostatic	−12.20	−10.85
Polar	11.11	10.36
Non-polar	−9.35	−10.74
Delta G gas	−41.3	−44.75
Delta G solv	−1.76	−0.38
Delta Total	−39.54	−45.13

### 3.3.4. DFT Studies of Bromobenzofuran-Oxadiazoles **BF1-9**

The energy computations of the three bioactive bromobenzofuran-oxadiazole analogues **BF-2**, **BF-5**, and **BF-6** were undertaken with the Gaussian calculation setups used in the optimization. From the DFT energy computation outcomes, the total energy, the HOMO energy, and the LUMO energy were calculated. By using the HOMO and LUMO energy figures, the other related parameters were calculated with the respective theorems, as presented in Table 9.

**Table 9.** The computed energy values and the related parameters for compounds **BF-2**, **BF-5** and **BF-6** (in eV).

Parameters	BF-2	BF-5	BF-6
$E_{\text{total}}$	−30,873.682	−36,325.869	−32,792.474
$E_{\text{HOMO}}$	−6.851	−6.163	−6.532
$E_{\text{LUMO}}$	−2.667	−2.444	−2.383
$\Delta E$	4.184	3.719	4.149
Ionization potential (IP = $-E_{\text{HOMO}}$ )	6.851	6.163	6.532
Electron affinity (A = $-E_{\text{LUMO}}$ )	2.667	2.444	2.383
Chemical potential ( $\mu = -(I + A)/2$ )	−4.759	−4.304	−4.458
Hardness ( $\eta = (I - A)/2$ )	2.092	1.860	2.075
Mulliken electronegativity ( $\chi = (I + A)/2$ ) [84]	4.759	4.304	−4.458
Softness ( $S = 1/2\eta$ )	0.239	0.269	0.241
Electrophilicity index ( $\omega = \mu^2/2\eta$ ) [85]	5.413	4.983	4.790
Maximum charge transfer ( $\Delta N_{\text{max}} = (I + A)/2(I - A)$ ) [86]	1.137	1.157	1.074

Both the HOMO and LUMO play an important role in estimating the electrical properties and chemical affinities of the bromobenzofuran-oxadiazole **BF-2**, **BF-5**, and **BF-6** compounds. The HOMO depicts the electron donors. On the other hand, the LUMO depicts the electron acceptors [87,88]. The HOMO energy value of compound **BF-5** was found to be the highest followed by the compounds **BF-6** and **BF-2**, respectively. Therefore, compound **BF-5** is expected to have the highest tendency to give electrons easily as depicted in Table 8. The HOMO–LUMO energy gap ( $\Delta E$ ) exhibits the chemical stability of compounds. A higher energy gap for a molecule implies higher chemical stability [89]. In the DFT study, compound **BF-2** had the highest energy gap among the three compounds. Hence, compound **BF-2** is expected to have the highest chemical stability. Global hardness depicts the resistance of an atom to electron transfer. Here, compound **BF-2** had the highest global hardness. From these outcomes of DFT analysis, it is inferred that bromobenzofuran-oxadiazole compound **BF-2** is the least reactive and has the highest chemical stability among the three bioactive **BF-2**, **BF-5**, and **BF-6** compounds [90]. The concentration of tubes for compound **BF-2** was around the benzofuran ring. On the other hand, for compound **BF-5**, the tubes were concentrated around the dimethoxyphenyl ring. The LUMO tubes for compound **BF-6** were concentrated around the benzofuran and the oxadiazole rings. However, its HOMO tubes were concentrated not only around the two heterocyclic structures but also around the fluoro phenyl ring, as presented in Figure 12. The DFT study revealed that the 2,5-dimethoxy-based benzofuran-oxadiazole **BF-5** can be the lead anti-HepG2 liver cancer structural motifs.

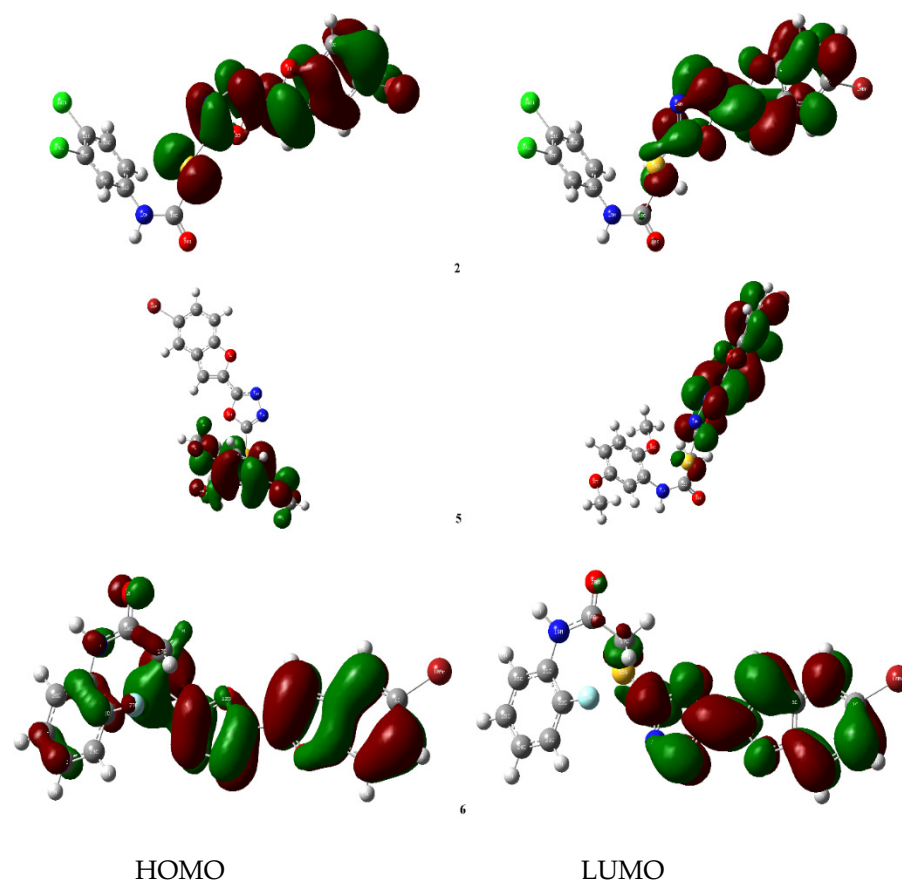


**Figure 12.** The HOMO (left) and LUMO (right) tube orientations of molecular orbitals of compounds **BF-2**, **BF-5**, and **BF-6**.

#### 4. Conclusions

In the present work, nine *S*-alkylated amide-linked bromobenzofuran-oxadiazole scaffolds **BF1-9** were achieved by employing the phase transfer catalyst BTEAC under the ultrasonic-assisted synthetic conditions in good yields (75–88%). These synthesized bromobenzofuran oxadiazoles **BF1-9** were evaluated for cytotoxic potential against human liver cancer cell line HepG2 and obtained promising results with cell viabilities of  $10.41 \pm 0.66\%$  to  $44.69 \pm 6.85\%$ . The least active 3,4-dimethyl containing benzofuran-oxadiazole **BF-9** showed maximum cell viability potential ( $44.69 \pm 6.85\%$ ), and the most bioactive 3,4-dimethoxy based benzofuran-oxadiazole demonstrated the minimum cell viability efficacy ( $10.41 \pm 0.66\%$ ) and excellent anti-HepG2 cytotoxic activity. The compounds 3,4-Dichloro-based **BF-2** ( $12.72 \pm 2.23\%$  cell viability) and 2-fluoro-based **BF-6** ( $13.08 \pm 1.08\%$  cell viability) displayed good cytotoxic potential. The cytotoxic therapeutic potential of **BF1-9** derivatives decreased in the following order: 2,5-dimethoxy > 3,4-dichloro > 2-fluoro > 4-fluoro > 2-methoxy > 2-chloro > phenyl > 2,4-dimethyl > 3,4-dimethyl. SAR revealed that the second and fourth positions of phenyl are responsible for the excellent anti-HepG2 cancer activity of benzofuran-oxadiazoles **BF1-9**, especially of 2,5-dimethoxy containing **BF-5** derivative. The EWGs such as methoxy, fluoro, and chloro on the second, fourth, and fifth positions of phenyl in the anilide ring of benzofuran-oxadiazoles **BF1-9** could enhance the cytotoxic potential while substituents pattern of the electron-donating groups (EDG) on the phenyl of anilide ring decreased the cytotoxic therapeutic potential of bromobenzofuran-oxadiazoles **BF1-9**. Furthermore, the *in silico* investigations for the identification of its probable mechanism of anti-cancer action revealed that these compounds showed good binding affinities and stable associations with the EGFR, PI3K, mTOR, and Tubulin polymerization enzymes. This study indicates that these four key enzymes may be the probable molecular targets for these compounds **BF1-9**. Based

on the significantly good binding affinities and associations, these in silico studies further validate the anti-HepG-2 cancer potential as witnessed in the in vitro evaluations. The novel **BF1-9** analogues did not demonstrate significant in silico results against the GSK-3 $\beta$  and AKT enzymes. The ADMET assessment demonstrated that novel bromobenzofuran-oxadiazoles **BF1-9** members have a high degree of drug-likeness profile. The DFT studies also revealed that bromobenzofuran-oxadiazole compound **BF-2** had the highest chemical stability while on the other hand, bromobenzofuran-oxadiazole structural motif **BF-5** was found to have the highest tendency to give its electrons easily as compared to **BF-2** and **BF-6**. All the in vitro and in silico findings of the present research work against anti-HepG-2 cancer cell line and four key enzymes EGFR, PI3K, mTOR, and Tubulin polymerization conclude that the 2,5-dimethoxy based bromobenzofuran-oxadiazole **BF-5** could be the potential lead anti-HepG2 cancer agent.

**Author Contributions:** Conceptualization, A.F.Z., M.E.A.Z. and A.I.; methodology, A.I. and R.N.; Biological Activity, A.R.; software, S.F., A.I., S.A. and M.T.M.; validation, S.F., S.A. and A.I.; formal analysis, S.F. and A.I. investigation, A.I.; resources, A.F.Z. and S.A.A.-H. data curation, S.A.A.-H. and R.N.; writing—original draft preparation, A.I.; writing—review and editing, A.I., S.F., A.F.Z. and M.E.A.Z. Visualization, A.I. and S.F.; supervision, A.F.Z.; project administration, A.F.Z. and M.E.A.Z. funding acquisition, S.A.A.-H., A.I. and M.E.A.Z. All authors have read and agreed to the published version of the manuscript.

**Funding:** This research was supported by the Deanship of Scientific Research, Imam Mohammad Ibn Saud Islamic University (IMSIU), Saudi Arabia.

**Institutional Review Board Statement:** Not applicable.

**Informed Consent Statement:** Not applicable.

**Data Availability Statement:** Data is available in the manuscript.

**Acknowledgments:** Authors acknowledge the Government college university Faisalabad for research facilities provided to carry out this research work.

**Conflicts of Interest:** The authors declare no conflict of interest.

## References

1. Siegel, R.; Naishadham, D.; Jemal, A. Cancer Statistics, 2013. *CA-Cancer J. Clin.* **2013**, *63*, 11–30. [[CrossRef](#)] [[PubMed](#)]
2. Rowinsky, E.K. The pursuit of optimal outcomes in cancer therapy in a new age of rationally designed target-based anticancer agents. *Drugs* **2000**, *60*, 1–14. [[CrossRef](#)]
3. Weinberg, R.A. How Cancer Arises. *Sci Am.* **1996**, *275*, 62–70. [[CrossRef](#)]
4. Johnson, D.S.; Li, J.J. *The Art of Drug Synthesis*; Wiley-Interscience: Hoboken, NJ, USA, 2007. [[CrossRef](#)]
5. Bray, F.; Ferlay, J.; Soerjomataram, I.; Siegel, R.L.; Torre, L.A.; Jemal, A. Global cancer statistics 2018: GLOBOCAN estimates of incidence and mortality worldwide for 36 cancers in 185 countries. *CA Cancer J. Clin.* **2018**, *68*, 394–424. [[CrossRef](#)]
6. Philips, C.A.; Rajesh, S.; Nair, D.C.; Ahamed, R.; Abduljaleel, J.K.; Augustine, P. Hepatocellular Carcinoma in 2021: An Exhaustive Update. *Cureus* **2021**, *13*, e19274. [[CrossRef](#)]
7. Suresh, D.; Srinivas, A.N.; Kumar, D.P. Etiology of Hepatocellular Carcinoma: Special Focus on Fatty Liver Disease. *Front. Oncol.* **2020**, *30*, 601710. [[CrossRef](#)]
8. Ferlay, J.; Colombet, M.; Soerjomataram, I.; Mathers, C.; Parkin, D.M.; Piñeros, M.; Znaor, A.; Bray, F. Estimating the global cancer incidence and mortality in 2018: GLOBOCAN sources and methods. *Int. J. Cancer.* **2019**, *144*, 1941–1953. [[CrossRef](#)] [[PubMed](#)]
9. Yang, J.D.; Hainaut, P.; Gores, G.J.; Amadou, A.; Plymoth, A.; Roberts, L.R. A global view of hepatocellular carcinoma: Trends, risk, prevention and management. *Nat. Rev. Gastroenterol. Hepatol.* **2019**, *16*, 589–604. [[CrossRef](#)] [[PubMed](#)]
10. Shahzadi, I.; Zahoor, A.F.; Parveen, B.; Rasul, A.; Raza, Z.; Ahmad, S.; Irfan, I.; El-Hiti, G.A. Acefylline Derivatives as a New Class of Anticancer Agents: Synthesis, Molecular Docking, and Anticancer, Hemolytic, and Thrombolytic Activities of Acefylline-Triazole Hybrids. *J. Chem.* **2022**, *2022*, 3502872. [[CrossRef](#)]
11. Sharma, R.A.; Plummer, R.; Stock, J.K.; Greenhalgh, T.A.; Ataman, O.; Kelly, S.; Clay, R.; Adams, R.A.; Baird, R.D.; Billingham, L.; et al. Clinical development of new drug-radiotherapy combinations. *Nat. Rev. Clin. Oncol.* **2016**, *13*, 627–642. [[CrossRef](#)] [[PubMed](#)]
12. Arruebo, M.; Vilaboa, N.; Sáez-Gutierrez, B.; Lambea, J.; Tres, A.; Valladares, M.; González-Fernández, A. Assessment of the evolution of cancer treatment therapies. *Cancers* **2011**, *3*, 3279–3330. [[CrossRef](#)] [[PubMed](#)]

13. Prachayasittikul, V.; Pingaew, R.; Anuwongcharoen, N.; Worachartcheewan, A.; Nantasenamat, C.; Prachayasittikul, S.; Ruchirawat, S.; Prachayasittikul, V. Discovery of novel 1,2,3-triazole derivatives as anticancer agents using QSAR and in silico structural modification. *SpringerPlus* **2015**, *4*, 571. [[CrossRef](#)] [[PubMed](#)]
14. Kapoor, G.; Bhutani, R.; Pathak, P.D.; Chauhan, G.; Kant, R.; Grover, P.; Nagarajan, K.; Siddiqui, S.A. Current Advancement in the Oxadiazole-Based Scaffolds as Anticancer Agents. *Polycycl. Aromat. Compd.* **2022**, *42*, 4183–4215. [[CrossRef](#)]
15. Aziz, H.; Zahoor, A.F.; Shahzadi, I.; Irfan, A. Recent Synthetic Methodologies Towards the Synthesis of Pyrazoles. *Polycycl. Aromat. Compd.* **2019**, *41*, 698–720. [[CrossRef](#)]
16. Sudeesh, K.; Gururaja, R. Facile synthesis of some novel derivatives of 1,3,4-oxadiazole derivatives associated with quinolone moiety as cytotoxic and antibacterial agents. *Org. Chem. Curr. Res.* **2017**, *6*, 2–5.
17. Nayak, S.; Gaonkar, S.L.; Musad, E.A.; Dawsar, A.M.A. 1,3,4-Oxadiazole-containing hybrids as potential anticancer agents: Recent developments, mechanism of action and structure-activity relationships. *J. Saudi Chem. Soc.* **2021**, *25*, 101284. [[CrossRef](#)]
18. Lelyukh, M.; Martynets, M.; Kalytovska, M.; Drapak, I.; Harkov, S.; Chaban, T.; Chaban, I.; Matiychuk, V. Approaches for synthesis and chemical modification of non-condensed heterocyclic systems based on 1,3,4-oxadiazole ring and their biological activity: A review. *J. Appl. Pharm. Sci.* **2020**, *10*, 151–165.
19. Luczynski, M.; Kudelko, A. Synthesis and Biological Activity of 1,3,4-Oxadiazoles Used in Medicine and Agriculture. *Appl. Sci.* **2022**, *12*, 3756. [[CrossRef](#)]
20. Napiórkowska, M.; Cieślak, M.; Barańska, K.J.; Golińska, K.K.; Nawrot, B. Synthesis of new derivatives of benzofuran as potential anticancer agents. *Molecules* **2019**, *24*, 1529. [[CrossRef](#)]
21. Radadiya, A.; Shah, A. Bioactive benzofuran derivatives: An insight on lead developments, radioligands and advances of the last decade. *Eur. J. Med. Chem.* **2015**, *97*, 356–376. [[CrossRef](#)]
22. Nevagi, R.J.; Dighe, S.N. Biological and medicinal significance of benzofuran. *Eur. J. Med. Chem.* **2014**, *97*, 561–581. [[CrossRef](#)] [[PubMed](#)]
23. Miao, Y.-H.; Hu, Y.-H.; Yang, J.; Liu, T.; Sun, J.; Wang, X.-J. Natural source, bioactivity and synthesis of benzofuran derivatives. *RSC Adv.* **2019**, *9*, 27510. [[CrossRef](#)]
24. Othman, D.I.; Abdelal, A.M.M.; El-Sayed, M.A.; El Bialy, S.A.A. Novel Benzofuran Derivatives: Synthesis and Antitumor Activity. *Heterocycl. Commun.* **2013**, *19*, 29–35. [[CrossRef](#)]
25. Abdelfatah, S.; Berg, A.; Huang, Q.; Yang, L.J.; Hamdoun, S.; Klinger, A.; Greten, H.J.; Fleischer, E.; Berg, T.; Wong, V.K.W.; et al. MCC1019, a Selective Inhibitor of the Polo-Box Domain of Polo-like Kinase 1 as Novel, Potent Anticancer Candidate. *Acta Pharm. Sin. B* **2019**, *9*, 1021–1034. [[CrossRef](#)] [[PubMed](#)]
26. Chen, Y.; Law, P.-Y.; Loh, H. Inhibition of PI3K/Akt Signaling: An Emerging Paradigm for Targeted Cancer Therapy. *Curr. Med. Chem. Agents.* **2005**, *5*, 575–589. [[CrossRef](#)]
27. Abdelhafez, O.M.; Amin, K.M.; Ali, H.I.; Abdalla, M.M.; Ahmed, E.Y. Design, Synthesis and Anticancer Activity of Benzofuran Derivatives Targeting VEGFR-2 Tyrosine Kinase. *RSC Adv.* **2014**, *4*, 11569–11579. [[CrossRef](#)]
28. El-Zahabi, M.A.; Sakr, H.; El-Adl, K.; Zayed, M.; Abdelraheem, A.S.; Eissa, S.I.; Elkady, H.; Eissa, I.H. Design, synthesis, and biological evaluation of new challenging thalidomide analogs as potential anticancer immunomodulatory agents. *Bioorg. Chem.* **2020**, *104*, 104218. [[CrossRef](#)]
29. Vaidya, A.; Pathak, D.; Shah, K. 1,3,4-oxadiazole and its derivatives: A review on recent progress in anticancer activities. *Chem. Biol. Drug Des.* **2021**, *97*, 572–591. [[CrossRef](#)] [[PubMed](#)]
30. Alam, M.M.; Nazreen, S.; Almalki, A.S.A.; Elhenawy, A.A.; Alsenani, N.I.; Elbehairi, S.E.I.; Malebari, A.M.; Alfaifi, M.Y.; Alsharif, M.A.; Alfaifi, S.Y.M. Naproxen Based 1,3,4-Oxadiazole Derivatives as EGFR Inhibitors: Design, Synthesis, Anticancer, and Computational Studies. *Pharmaceuticals* **2021**, *14*, 870. [[CrossRef](#)]
31. Sankhe, N.M.; Durgashivaprasad, E.; Kutty, N.G.; Rao, J.V.; Narayanan, K.; Kumar, N.; Jain, P.; Udupa, N.; Palanimuthu, V.R. Novel 2,5-disubstituted-1,3,4-oxadiazole derivatives induce apoptosis in HepG2 cells through p53 mediated intrinsic pathway. *Arab. J. Chem.* **2019**, *12*, 2548–2555. [[CrossRef](#)]
32. Mohan, C.D.; Anilkumar, N.C.; Rangappa, S.; Shanmugam, M.K.; Mishra, S.; Chinnathambi, A.; Alharbi, S.A.; Bhattacharjee, A.; Sethi, G.; Kumar, A.P.; et al. Novel 1,3,4-Oxadiazole Induces Anticancer Activity by Targeting NF- $\kappa$ B in Hepatocellular Carcinoma Cells. *Front. Oncol.* **2018**, *8*, 42. [[CrossRef](#)]
33. Hagra, M.; Saleh, M.A.; Eldin, R.R.E.; Abuelkhir, A.A.; Khidr, E.G.; El-Husseiny, A.A.; El-Mahdy, H.A.; Elkaeed, E.B.; Eissa, I.H. 1,3,4-Oxadiazole-naphthalene hybrids as potential VEGFR-2 inhibitors: design, synthesis, antiproliferative activity, apoptotic effect, and in-silico studies. *J. Enzym. Inhib. Med. Chem.* **2022**, *37*, 386–402. [[CrossRef](#)]
34. Kassem, A.F.; Nassar, I.F.; Abdel-Aal, M.T.; Awad, H.M.; El-Sayed, W.A. Synthesis and Anticancer Activity of New ((Furan-2-yl)-1,3,4-thiadiazolyl)-1,3,4-oxadiazole Acyclic Sugar Derivatives. *Chem. Pharm. Bull.* **2019**, *67*, 888–895. [[CrossRef](#)] [[PubMed](#)]
35. Faiz, S.; Zahoor, A.F.; Ajmal, M.; Kamal, S.; Ahmad, S.; Abdelgawad, A.M.; Elnaggar, M.E. Design, Synthesis, Antimicrobial Evaluation, and Laccase Catalysis Effect of Novel Benzofuran-Oxadiazole and Benzofuran-Triazole Hybrids. *J. Heterocycl. Chem.* **2019**, *56*, 2839–2852. [[CrossRef](#)]
36. Irfan, A.; Faiz, S.; Rasul, A.; Zafar, R.; Zahoor, A.F.; Kotwica-Mojzych, K.; Mojzych, M. Exploring the Synergistic Anticancer Potential of Benzofuran-Oxadiazoles and Triazoles: Improved Ultrasound-and Microwave-Assisted Synthesis, Molecular Docking, Hemolytic, Thrombolytic and Anticancer Evaluation of Furan-Based Molecules. *Molecules* **2022**, *27*, 1023. [[CrossRef](#)]

37. Majumdar, C.K.; Biswas, A.; Mukhopadhyay, P.P. Carbon–Carbon Bond Formation by Radical Cyclisation: Regioselective Synthesis of Coumarin-Annulated Sulfur Heterocycles. *Synthesis* **2003**, *15*, 2385–2389. [[CrossRef](#)]
38. Majumdar, C.K.; Biswas, A. Regioselective Synthesis of Thieno[3,2-c][1]benzopyran-4-ones by Thio-Claisen Rearrangement. *Mon. Für Chem.* **2004**, *135*, 1001–1007. [[CrossRef](#)]
39. Irfan, A.; Zahoor, A.F.; Kamal, S.; Hassan, M.; Kloczkowski, A. Ultrasonic-Assisted Synthesis of Benzofuran Appended Oxadiazole Molecules as Tyrosinase Inhibitors: Mechanistic Approach through Enzyme Inhibition, Molecular Docking, Chemoinformatics, ADMET and Drug-Likeness Studies. *Int. J. Mol. Sci.* **2022**, *23*, 10979. [[CrossRef](#)] [[PubMed](#)]
40. Shahzadi, I.; Zahoor, A.F.; Rasul, A.; Rasool, N.; Raza, Z.; Faisal, S.; Parveen, B.; Kamal, S.; Zia-ur-Rehman, M.; Zahid, F.M. Synthesis, anticancer, and computational studies of 1, 3, 4-oxadiazole-purine derivatives. *Heterocycl. Chem.* **2020**, *57*, 2782–2794. [[CrossRef](#)]
41. Akhtar, R.; Zahoor, A.F.; Rasul, A.; Khan, S.G.; Ali, K.G. In-vitro cytotoxic evaluation of newly designed ciprofloxacin-oxadiazole hybrids against human liver tumor cell line (Huh7). *Pak. J. Pharm. Sci.* **2021**, *34*, 1143–1148.
42. Burley, S.K.; Berman, H.M.; Bhikadiya, C.; Bi, C.; Chen, L.; Di Costanzo, L.; Christie, C.; Dalenberg, K.; Duarte, J.M.; Dutta, S.; et al. RCSB Protein Data Bank: Biological Macromolecular Structures Enabling Research and Education in Fundamental Biology, Biomedicine, Biotechnology and Energy. *Nucleic Acids Res.* **2019**, *47*, D464–D474. [[CrossRef](#)] [[PubMed](#)]
43. Park, J.H.; Liu, Y.; Lemmon, M.A.; Radhakrishnan, R. Erlotinib Binds Both Inactive and Active Conformations of the EGFR Tyrosine Kinase Domain. *Biochem. J.* **2012**, *448*, 417–423. [[CrossRef](#)] [[PubMed](#)]
44. Cheng, H.; Li, C.; Bailey, S.; Baxi, S.M.; Goulet, L.; Guo, L.; Hoffman, J.; Jiang, Y.; Johnson, T.O.; Johnson, T.W.; et al. Discovery of the Highly Potent PI3K/MTOR Dual Inhibitor PF-04979064 through Structure-Based Drug Design. *ACS Med. Chem. Lett.* **2013**, *4*, 91–97. [[CrossRef](#)]
45. Buonfiglio, R.; Prati, F.; Bischetti, M.; Cavarischia, C.; Furlotti, G.; Ombrato, R. Discovery of Novel Imidazopyridine GSK-3 $\beta$  Inhibitors Supported by Computational Approaches. *Molecules* **2020**, *25*, 2163. [[CrossRef](#)]
46. Kallan, N.C.; Spencer, K.L.; Blake, J.F.; Xu, R.; Heizer, J.; Bencsik, J.R.; Mitchell, I.S.; Gloor, S.L.; Martinson, M.; Risom, T.; et al. Discovery and SAR of spirochromane Akt inhibitors. *Bioorg. Med. Chem. Lett.* **2011**, *21*, 2410–2414. [[CrossRef](#)]
47. Yang, H.; Rudge, D.G.; Koos, J.D.; Vaidialingam, B.; Yang, H.J.; Pavletich, N.P. mTOR kinase structure, mechanism and regulation. *Nature* **2013**, *497*, 217–223. [[CrossRef](#)] [[PubMed](#)]
48. Prota, A.E.; Danel, F.; Bachmann, F.; Bargsten, K.; Buey, R.M.; Pohlmann, J.; Reinelt, S.; Lane, H.; Steinmetz, M.O. The novel microtubule-destabilizing drug BAL27862 binds to the colchicine site of tubulin with distinct effects on microtubule organization. *J. Mol. Biol.* **2014**, *426*, 1848–1860. [[CrossRef](#)]
49. Vilar, S.; Cozza, G.; Moro, S. Medicinal Chemistry and the Molecular Operating Environment (MOE): Application of QSAR and Molecular Docking to Drug Discovery. *Curr. Top. Med. Chem.* **2008**, *8*, 1555–1572. [[CrossRef](#)]
50. Faisal, S.; Lal Badshah, S.; Kubra, B.; Sharaf, M.; Emwas, A.H.; Jaremko, M.; Abdalla, M. Computational Study of SARS-CoV-2 Rna Dependent Rna Polymerase Allosteric Site Inhibition. *Molecules* **2022**, *27*, 223. [[CrossRef](#)]
51. Studio, A.D. *Discovery Studio Modeling Environment, Release 3.5*; Accelrys Software Inc.: San Diego, CA, USA, 2012.
52. Mills, N. ChemDraw Ultra 10.0 CambridgeSoft, 100 CambridgePark Drive, Cambridge, MA 02140. www.cambridgesoft.com. Commercial Price: \$1910 for Download, \$2150 for CD-ROM; Academic Price: \$710 for Download, \$800 for CD-ROM. *J. Am. Chem. Soc.* **2006**, *128*, 13649–13650. [[CrossRef](#)]
53. Daina, A.; Michielin, O.; Zoete, V. SwissADME: A Free Web Tool to Evaluate Pharmacokinetics, Drug-Likeness and Medicinal Chemistry Friendliness of Small Molecules. *Sci. Rep.* **2017**, *7*, 42717. [[CrossRef](#)] [[PubMed](#)]
54. Xiong, G.; Wu, Z.; Yi, J.; Fu, L.; Yang, Z.; Hsieh, C.; Yin, M.; Zeng, X.; Wu, C.; Lu, A.; et al. ADMETlab 2.0: An Integrated Online Platform for Accurate and Comprehensive Predictions of ADMET Properties. *Nucleic Acids Res.* **2021**, *49*, W5–W14. [[CrossRef](#)] [[PubMed](#)]
55. Yang, H.; Lou, C.; Sun, L.; Li, J.; Cai, Y.; Wang, Z.; Li, W.; Liu, G.; Tang, Y. AdmetSAR 2.0: Web-Service for Prediction and Optimization of Chemical ADMET Properties. *Bioinformatics* **2019**, *35*, 1067–1069. [[CrossRef](#)] [[PubMed](#)]
56. Cheng, F.; Li, W.; Zhou, Y.; Shen, J.; Wu, Z.; Liu, G.; Lee, P.W.; Tang, Y. AdmetSAR: A Comprehensive Source and Free Tool for Assessment of Chemical ADMET Properties. *J. Chem. Inf. Model.* **2012**, *52*, 3099–3105. [[CrossRef](#)] [[PubMed](#)]
57. Case, D.A.; Aktulga, H.M.; Belfon, K.; Ben-Shalom, I.; Brozell, S.R.; Cerutti, D.S.; Cheatham, T.E., III; Cruzeiro, V.W.D.; Darden, T.A.; Duke, R.E.; et al. *Amber 2021*; University of California: San Francisco, CA, USA, 2021.
58. Wang, J.; Wang, W.; Kollman, P.A.; Case, D.A. Antechamber: An accessory software package for molecular mechanical calculations. *J. Am. Chem. Soc.* **2001**, *222*, 1–41.
59. Wickstrom, L.; Hauser, K.E.; Simmerling, C. ff14SB: Improving the accuracy of protein side chain and backbone parameters from ff99SB. *J. Chem. Theory Comput.* **2015**, *11*, 3696–3713.
60. Sprenger, K.G.; Jaeger, V.W.; Pfaendtner, J. The general AMBER force field (GAFF) can accurately predict thermodynamic and transport properties of many ionic liquids. *J. Phys. Chem. B* **2015**, *119*, 5882–5895. [[CrossRef](#)]
61. Roe, D.R.; Cheatham, T.E., III. PTRAJ and CPPTRAJ: Software for processing and analysis of molecular dynamics trajectory data. *J. Chem. Theory Comput.* **2013**, *9*, 3084–3095. [[CrossRef](#)]
62. Miller, B.R., III; McGee, T.D., Jr.; Swails, J.M.; Homeyer, N.; Gohlke, H.; Roitberg, A.E. MMPBSA. py: An efficient program for end-state free energy calculations. *J. Chem. Theory Comput.* **2012**, *8*, 3314–3321. [[CrossRef](#)]

63. Genheden, S.; Ryde, U. The MM/PBSA and MM/GBSA methods to estimate ligand-binding affinities. *Expert Opin. Drug Discov.* **2015**, *10*, 449–461. [[CrossRef](#)]
64. Frisch, M.J.; Trucks, G.W.; Schlegel, H.B.; Scuseria, G.E.; Robb, M.A.; Cheeseman, J.R.; Scalmani, G.; Barone, V.; Petersson, G.A.; Nakatsuji, H.; et al. Gaussian. *J. Nat. Sci. Ed.* **2009**, *09*, 53–54.
65. Becke, A.D. Density-functional thermochemistry. IV. A new dynamical correlation functional and implications for exact-exchange mixing. *J. Chem. Phys.* **1996**, *104*, 1040–1046. [[CrossRef](#)]
66. Perdew, J.P.; Kurth, S. Accurate density functional with correct formal properties: A step beyond the generalized gradient approximation. *Phys. Rev. Lett.* **1999**, *82*, 2544–2547. [[CrossRef](#)]
67. Dennington, J.M.; Keith, R.D.; Millam, T.A. *GaussView 5.0*, Semichem Inc.: Shawnee Mission, KS, USA, 2008.
68. Zhang, C.; Peng, L.; Zhang, Y.; Liu, Z.; Li, W.; Chen, S.; Li, G. The Identification of Key Genes and Pathways in Hepatocellular Carcinoma by Bioinformatics Analysis of High-Throughput Data. *Med. Oncol.* **2017**, *34*, 101. [[CrossRef](#)] [[PubMed](#)]
69. Juaid, N.; Amin, A.; Abdalla, A.; Reese, K.; Alamri, Z.; Moulay, M.; Abdu, S.; Miled, N. Anti-Hepatocellular Carcinoma Biomolecules: Molecular Targets Insights. *Int. J. Mol. Sci.* **2021**, *22*, 10774. [[CrossRef](#)] [[PubMed](#)]
70. Zhou, L.; Du, Y.; Kong, L.; Zhang, X.; Chen, Q. Identification of Molecular Target Genes and Key Pathways in Hepatocellular Carcinoma by Bioinformatics Analysis. *Onco. Targets. Ther.* **2018**, *11*, 1861–1869. [[CrossRef](#)]
71. Zhu, M.; Li, W.; Lu, Y.; Dong, X.; Lin, B.; Chen, Y.; Zhang, X.; Guo, J.; Li, M. HBx Drives Alpha Fetoprotein Expression to Promote Initiation of Liver Cancer Stem Cells through Activating PI3K/AKT Signal Pathway. *Int. J. Cancer* **2017**, *140*, 1346–1355. [[CrossRef](#)]
72. Tsai, K.H.; Hsien, H.H.; Chen, L.M.; Ting, W.J.; Yang, Y.S.; Kuo, C.H.; Tsai, C.H.; Tsai, F.J.; Tsai, H.J.; Huang, C.Y. Rhubarb Inhibits Hepatocellular Carcinoma Cell Metastasis via GSK-3- $\beta$  Activation to Enhance Protein Degradation and Attenuate Nuclear Translocation of  $\beta$ -Catenin. *Food Chem.* **2013**, *138*, 278–285. [[CrossRef](#)]
73. Mancinelli, R.; Carpino, G.; Petrunaro, S.; Mammola, C.L.; Tomaipitina, L.; Filippini, A.; Facchiano, A.; Ziparo, E.; Giampietri, C. Multifaceted Roles of GSK-3 in Cancer and Autophagy-Related Diseases. *Oxid. Med. Cell. Longev.* **2017**, *2017*, 4629495.
74. Hindson, J. Lenvatinib plus EGFR Inhibition for Liver Cancer. *Nat. Rev. Gastroenterol. Hepatol.* **2021**, *18*, 675. [[CrossRef](#)]
75. Abbas, H.A.S.; Abd El-Karim, S.S. Design, Synthesis and Anticancer Activity of New Benzofuran–Pyrazol–Hydrazono–Thiazolidin-4-One Hybrids as Potential EGFR Inhibitors and Apoptosis Inducing Agents. *Bioorg. Chem.* **2019**, *89*, 103035. [[CrossRef](#)]
76. Mphahlele, M.J.; Maluleka, M.M.; Parbhoo, N.; Malindisa, S.T. Synthesis, Evaluation for Cytotoxicity and Molecular Docking Studies of Benzo[c]Furan-Chalcones for Potential to Inhibit Tubulin Polymerization and/or EGFR-Tyrosine Kinase Phosphorylation. *Int. J. Mol. Sci.* **2018**, *19*, 2552. [[CrossRef](#)]
77. Mervai, Z.; Reszegi, A.; Miklya, I.; Knoll, J.; Schaff, Z.; Kovalszky, I.; Baghy, K. Inhibitory Effect of (2R)-1-(1-Benzofuran-2-Yl)-N-Propylpentan-2-Amine on Lung Adenocarcinoma. *Pathol. Oncol. Res.* **2020**, *26*, 727–734. [[CrossRef](#)]
78. Saitoh, M.; Kunitomo, J.; Kimura, E.; Iwashita, H.; Uno, Y.; Onishi, T.; Uchiyama, N.; Kawamoto, T.; Tanaka, T.; Mol, C.D.; et al. 2-[3-[4-(Alkylsulfanyl)Phenyl]-1-Benzofuran-5-Yl]-5-Methyl-1,3,4-Oxadiazole Derivatives as Novel Inhibitors of Glycogen Synthase Kinase-3 $\beta$  with Good Brain Permeability. *J. Med. Chem.* **2009**, *52*, 6270–6286. [[CrossRef](#)] [[PubMed](#)]
79. Eldehna, W.M.; Al-Rashood, S.T.; Al-Warhi, T.; Eskandrani, R.O.; Alharbi, A.; El Kerdawy, A.M. Novel Oxindole/Benzofuran Hybrids as Potential Dual CDK2/GSK-3 $\beta$  Inhibitors Targeting Breast Cancer: Design, Synthesis, Biological Evaluation, and in Silico Studies. *J. Enzyme Inhib. Med. Chem.* **2021**, *36*, 270–285. [[CrossRef](#)]
80. Gaisina, I.N.; Gallier, F.; Ougolkov, A.V.; Kim, K.H.; Kurome, T.; Guo, S.; Holzle, D.; Luchini, D.N.; Blond, S.Y.; Billadeau, D.D.; et al. From a Natural Product Lead to the Identification of Potent and Selective Benzofuran-3-Yl-(Indol-3-Yl)Maleimides as Glycogen Synthase Kinase 3 $\beta$ inhibitors That Suppress Proliferation and Survival of Pancreatic Cancer Cells. *J. Med. Chem.* **2009**, *52*, 1853–1863. [[CrossRef](#)]
81. El-Khouly, O.A.; Henen, M.A.; El-Sayed, M.A.A.; Shabaan, M.I.; El-Messery, S.M. Synthesis, Anticancer and Antimicrobial Evaluation of New Benzofuran Based Derivatives: PI3K Inhibition, Quorum Sensing and Molecular Modeling Study. *Bioorganic Med. Chem.* **2021**, *31*, 115976. [[CrossRef](#)] [[PubMed](#)]
82. Gao, Y.; Ma, C.; Feng, X.; Liu, Y.; Haimiti, X. BF12, a Novel Benzofuran, Exhibits Antitumor Activity by Inhibiting Microtubules and the PI3K/Akt/MTOR Signaling Pathway in Human Cervical Cancer Cells. *Chem. Biodivers.* **2020**, *17*, e1900622. [[CrossRef](#)] [[PubMed](#)]
83. Farhat, J.; Alzyoud, L.; Alwahsh, M.; Al-Omari, B. Structure–Activity Relationship of Benzofuran Derivatives with Potential Anticancer Activity. *Cancers* **2022**, *14*, 2196. [[CrossRef](#)] [[PubMed](#)]
84. Parr, R.G.; Donnelly, R.A.; Levy, M.; Palke, W.E. Electronegativity: The density functional viewpoint. *J. Chem. Phys.* **1978**, *68*, 3801. [[CrossRef](#)]
85. Chattaraj, P.K.; Sarkar, U.; Roy, D.R. Electrophilicity index. *Chem. Rev.* **2006**, *106*, 2065–2091. [[CrossRef](#)]
86. Koopmans, T. About the assignment of wave functions and eigenvalues to the individual electrons of an atom. *Physica* **1934**, *1*, 104–113. [[CrossRef](#)]
87. Miar, M.; Shiroudi, A.; Pourshamsian, K.; Oliay, A.R.; Hatamjafari, F. Theoretical investigations on the HOMO–LUMO gap and global reactivity descriptor studies, natural bond orbital, and nucleus-independent chemical shifts analyses of 3-phenylbenzo[d]thiazole-2(3H)-imine and its para-substituted derivatives: Solvent and subs. *J. Chem. Res.* **2021**, *45*, 147–158. [[CrossRef](#)]

88. Akkoc, S.; Karatas, H.; Muhammed, M.T.; Ceylan, A.; Almalki, F.; Laaroussi, H.; Ben, T.; Laaroussi, H.; Ben Hadda, T. Drug design of new therapeutic agents: Molecular docking, molecular dynamics simulation, DFT and POM analyses of new Schiff base ligands and impact of substituents on bioactivity of their potential antifungal pharmacophore site. *J. Biomol. Struct. Dyn.* **2022**, 1–14. [[CrossRef](#)] [[PubMed](#)]
89. Ruiz-Morales, Y. HOMO-LUMO gap as an index of molecular size and structure for polycyclic aromatic hydrocarbons (PAHs) and asphaltenes: A theoretical study. I. *J. Phys. Chem. A* **2002**, 106, 11283–11308. [[CrossRef](#)]
90. Han, M.İ.; Dengiz, C.; Doğan, Ş.D.; Gündüz, M.G.; Köprü, S.; Özkul, C. Isoquinolinedione-urea hybrids: Synthesis, antibacterial evaluation, drug-likeness, molecular docking and DFT studies. *J. Mol. Struct.* **2022**, 1252, 132007. [[CrossRef](#)]

**Disclaimer/Publisher's Note:** The statements, opinions and data contained in all publications are solely those of the individual author(s) and contributor(s) and not of MDPI and/or the editor(s). MDPI and/or the editor(s) disclaim responsibility for any injury to people or property resulting from any ideas, methods, instructions or products referred to in the content.